Geopersia 2021, 11(1): 169-203
DOI: 10.22059/GEOPE.2020.301603.648548

RESEARCH PAPER

The Sedimentological Record of Upper Holocene Tsunami Event in Fengbin, Taiwan

Fx Anjar Tri Laksono [1,*], Louis Loung-Yie Tsai [2], Jessica E. Pilarczyk [3]

[1] Department of Geological Engineering, Jenderal Soedirman University, Kalimanah, Purbalingga, Indonesia
[2] Graduate Institute of Applied Geology, National Central University, Taoyuan, Taiwan
[3] Department of Earth Sciences, Simon Fraser University, Burnaby, B.C. Canada

Received: 25 April 2020, Revised: 26 August 2020, Accepted: 21 September 2020

Abstract
A tsunami had struck the Ami tribe's settlement on the eastern coast of Taiwan in 1771. The trigger of this tsunami is still debatable. Hence, the analysis of tsunami deposits in Fengbin is needed to understand the chronology of the tsunami. There are three types of sediment samples taken from the study area, namely modern beach sand, modern fluvial sand, and sediment materials from the marine terrace. Sample analysis was carried out using the point counting, granulometry, biozonation, and paleo-bathymetry methods to determine the facies, provenance, and sediment transport mechanisms. The results of field observation indicate the presence of marine shells on the sediment deposit of marine terraces at elevations between 10.5-12.5 m. The thickness of this deposit is between 15-20 cm in the fining upward succession and there is a rip-up clast sedimentary structure. The characteristic of this deposit is similar to tsunami deposits found on the Ishigaki and Miyako Islands, Japan. The conclusion of this study is that there is a tsunami deposit in Fengbin associated with the tsunami deposits found in Miyako and Ishigaki Islands, Japan. The trigger of the tsunami in Fengbin probably attributed to tectonic activity in the Ryukyu Trench.

Keywords: Paleo-Tsunami, Upper Holocene, Marine Terrace, Sedimentological Record, Fengbin.

Introduction

Eastern Taiwan has experienced major earthquakes (Mw > 7). According to Ami's folklore, one of the Taiwanese aboriginal tribes-,"a high sea wave hit the Chenggong area in 1771 AD". This tragedy induced damage to their settlement (Abe, 1938). It had a run-up of at least 18 m above sea-level and inundation distance around 400 m from the shoreline (Ando et al., 2013). Nevertheless, Ami's people in Hualien, around 100 km northward of Chenggong never have any folklore related to this event. The absence of a story about this tragedy in areas nearby Chenggong is possibly due to Ami who lived in a lower elevation than others (Ando et al., 2013).

Based on a numerical simulation which was conducted by Ando et al. (2013), this tragedy occurred in the middle of the 18th century. They used numerical simulation to examine the possibility of impact 1771 tsunami in Miyako and Ishigaki Islands to the high sea wave events on the eastern coast of Taiwan. Ando et al. (2013) make a conclusion that the tsunami wave in 1771 can reach the eastern coast of Taiwan. The trigger of the 1771 tsunami in Miyako and Ishigaki Islands was a submarine landslide in the Ryukyu Trench (Fig. 1) (Ando et al., 2013).

* Corresponding author e-mail: anjar.trilaksono@unsoed.ac.id

Nonetheless, the evidence supporting their hypothesis is still considerably less. Moreover, they never consider longshore current on eastern Taiwan offshore. Another possibility is high sea waves because of the typhoon as claimed by Lallemand et al. (2016).

According to Lallemand et al. (2016), on the top of the Changbin High, at 1203 m of water depth, 20 km off the east coast of Taiwan, at a location sheltered from turbidity currents, they discovered a 23 cm thick anomalous sequence of silty material topped with a transported fragment of shells and wood interbedded with clay hemipelagites. This multiple-event has been dated between 1139 ± 140 cal BC (basalt layer) and 1056 ± 78 cal BC (top layer). There are multiple-events characterized by four distinct turbidite silty layers and one top deposit made of shallow-marine shells and wood debris without significant silty component. Four lower layers exhibit events generated by nearby submarine landslide were probably triggered by clustered earthquakes, then a super typhoon or tsunami occurred, resulting in shells and wood fragments deposit.

Furthermore, Ota et al. (2015) found six sites with large coral boulders on the surface of Holocene coral reef terraces. According to the ages of the coral boulders, it is possible that tsunami occurred several times since the mid-Holocene high stand of sea-level. The youngest event occurred some 100-170 years ago. This event can correlate with the 1771 Meiwa tsunami of the southern Ryukyu Islands. The locations of the coral boulder along the northern coast of the Lanyu Island suggest that the sources of the events are located to the north of the island. Three coral boulders (approximately 5 m across) were found resting on the Holocene coral terrace on the Jiupeng coast of southeastern Taiwan. Three exotic corals on the outer part of the boulders are dated at ca. 5000 year BP (before present) which is similar to that of insitu corals composing the Holocene terrace. These boulders were broken off from the coral terrace and were transported by tsunami waves (Matta et al., 2013).

A recent study which was conducted by Ando et al. (2018) expressed that there are four paleo-tsunami deposits in Ishigaki (Fig. 1) and Miyako Islands, Japan. Based on carbon dating, their deposits are from tsunami events in the past 2000 years. One of the greatest sea-level tsunamis in this place occurred in 1771. The trigger of this event is thrust fault at the Ryukyu subduction zone (Fig. 1). The maximum run-up of this tragedy reaches 30 m. The recurrence interval of tsunami events at the Ryukyu subduction zone is roughly 600 years. However, some previous tsunami studies did not find tsunami deposits on the eastern coast of Taiwan. Based on a numerical simulation which is proposed by Ando et al. (2013), tsunami waves can reach the eastern coast of Taiwan. Previous studies about strong sea wave events on the eastern coast of Taiwan are summarized briefly in Table 1.

We observed the coastal terrace along Fengbin (Fig. 2), then try to understand the facies of deposits in this study area. Determination of facies is very important for knowing geological processes that occur in the past including extreme events such as tsunami, storm, and sea-level change. The aims of this study are to discover and analyze tsunami deposits thus the chronology of the tsunami can be known.

Table 1. Previous studies and references for the strong sea wave event on the eastern coast of Taiwan

Previous research conclusions	References
Chenggong tsunami occurred in 1771. It was related to the 1771 tsunami south of Ishigaki Island.	Ando et al., 2013
Three coral boulders were found resting on the Holocene coral terrace on the Jiupeng coast.	Matta et al., 2013
Paleotsunamis took place several times since the mid-Holocene high stand of sea-level.	Ota et al., 2015
The strong sea wave events in Chenggong area was storm.	Lallemand at al., 2016.
Four paleotsunami deposits were discovered on the coastal lowland north of the southern Ryukyu subduction zone trench.	Ando et al., 2018

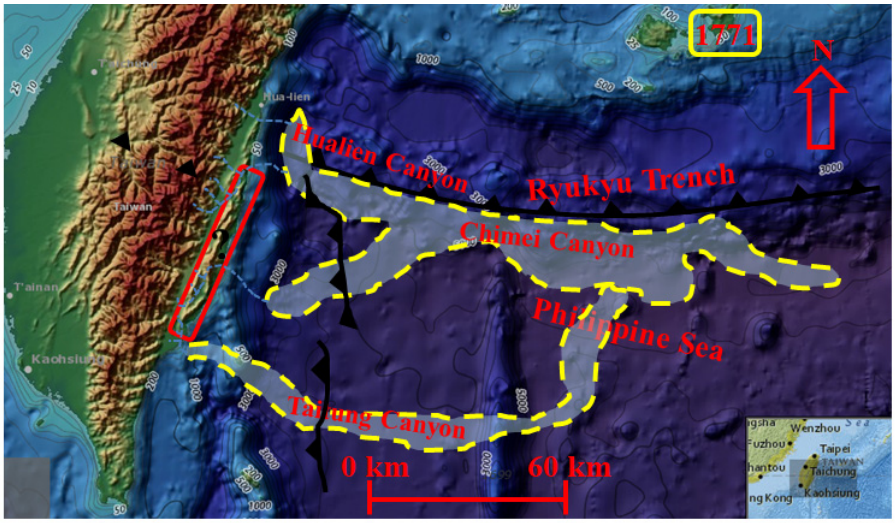

Figure 1. The tectonic setting of eastern Taiwan. Red square: study area in this research, yellow box: Ishigaki Island, black line with triangles: thrust fault at the subduction zone of Ryukyu Trench. The year 1771 is one of the tsunami events in Japan (Lehu et al., 2015)

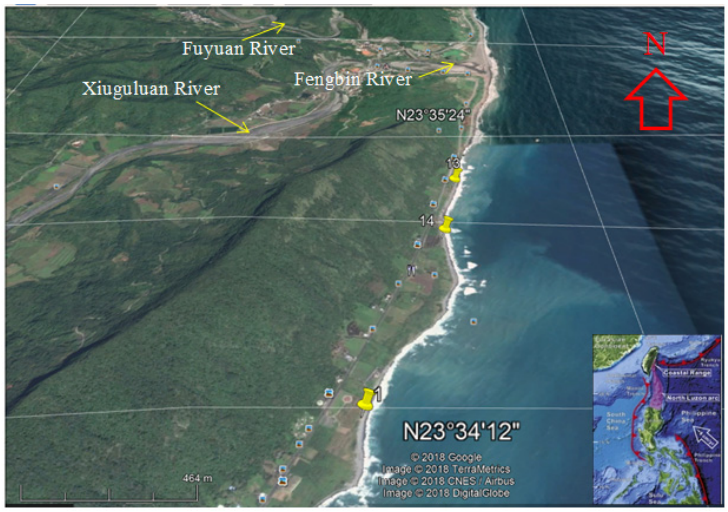

Figure 2. Location of study area in Fengbin (Google Earth). The numbers depict sampling sites (SS) in this study

Geological Setting

Regional Geology of Coastal Range

Taiwan Island was formed by the convergence between the Philippine Sea Plate and China continental margin which is a part of the Eurasian Plate (Teng, 1990). The convergence rate reaches to 80 mm/year northward. In the south of Taiwan and China sea, Eurasian Plate converges beneath Philippine Sea Plate. However, in the northeast of Taiwan Island, Philippine Sea Plate truncates beneath Eurasian Plate because there is an opening Okinawa Trough (Biq, 1972; Suppe, 1984).

In the eastern Coastal Range, Ryukyu subduction extends to the Honshu Island in Japan (Song & Lo, 1988) Although having a high subduction rate (47-104 mm/yr), for about a century it just yielded a few earthquakes with moment magnitude scale (Mw) > 8, that happened in northern of Nankai Trough (Matta et al., 2013). Meanwhile, there was no Mw > 8 earthquake

on the eastern coast of Taiwan in the last century (Ando, 1975). One of the earthquake events on the eastern coast of Taiwan induced by subduction of the Ryukyu arc and Okinawa Trough occurred in 1771 (Ma & Lee, 1997). Ando et al. (2013) suggested this earthquake had caused a big sea wave and destroyed the settlement of the Ami tribe in Chenggong.

Based on the geodetic data and radiometric dates at marine terraces along Hualien to Taitung, the uplift rate of the Coastal Range is approximately 12 mm/yr on average (Chen et al., 1991). Nevertheless, the uplift rate in one place with other places is not the same (Chen, 1984; Liu & Yu, 1990). The northernmost 30 km of the coast from the Takeng to Hsinshe has uplift rates of less than 4 mm/yr (Fig. 3) (Liew et al., 1990).

In the Fengbin area, the uplift rate is around 5 mm/yr. The central 30 km long coast southward to Pahsientung is uplifted more uniformly with rates 4–7 mm/yr (Liew et al., 1993). Yamaguchi & Ota (2004) specifically mentioned that the uplift rate in Changbin marine terrace is approximately 6 mm/yr. Southward, the remaining 80 km long coast is generally uplifted at 7–10 mm/yr, with local troughs (about 5 km in length and < 4 mm/yr in uplift rate) occurring around the mouth of the Sanhsien River and around Duli (Chen et al., 1991).

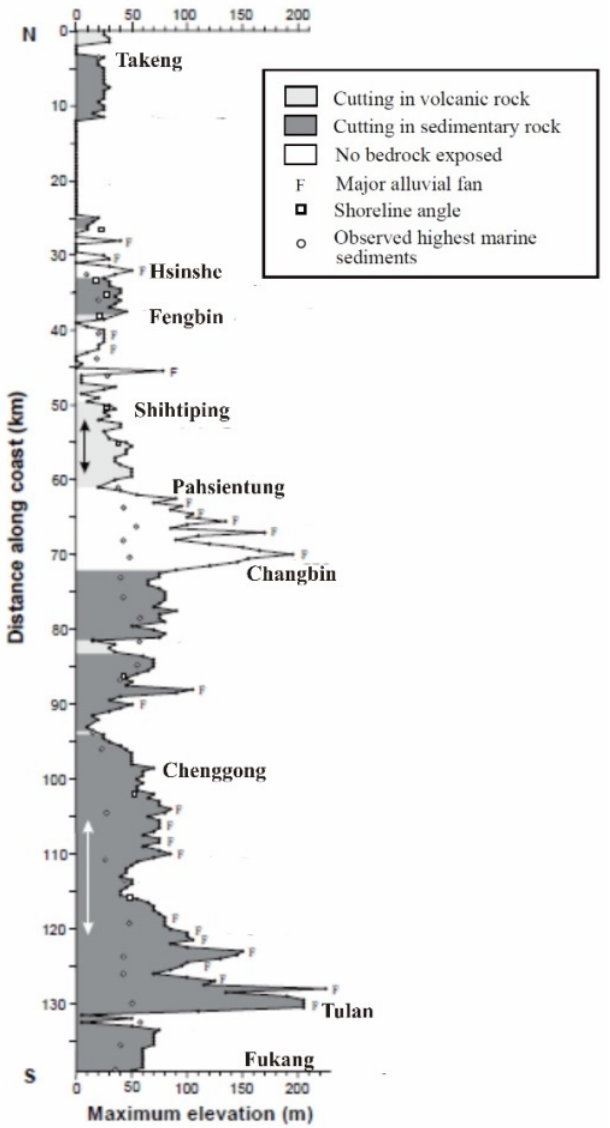

Figure 3. Morphology of marine terraces througout Takeng to Fukang. Based on this figure, the highest elevation lies in Tulan (Hsieh et al., 2004)

The crest of the uplift, with rates greater than 10 mm/yr, is probably located between Tulan and Fukang in the southernmost of the coast (Hsieh et al., 2004). The more specific hypothesis is expressed by Hsieh & Rau (2009), the uplift rate of the marine terrace in Tulan reaches 7.6 mm/yr.

Based on a topographic map (Fig. 4), there are three morphologies from the eastern coast of Taiwan to central Taiwan, namely Central Range, Longitudinal Valley, and Coastal Range (Wang et al., 1992). The Coastal Range extends from the north (Hualien) to the south (Taitung) along 150 km and a width of about 12 km (Hsieh & Rau, 2009). The uplift rate of the Coastal Range is not uniform (Hsieh et al., 2004). In the middle and southern parts of Coastal Range slightly more rapid than the northern part of Coastal Range (Hsieh et al., 2004; Hsieh & Rau, 2009). The Coastal Range and the Central Range is separated by a Longitudinal Valley with a width of 4 km (Hsieh et al., 2004).

The bathymetric map (Fig. 5) shows that the morphology of eastern Taiwan from the shoreline to 40 km seaward along Changbin to Taitung can be divided into 5 sections: Marine Terrace, Changbin High, Takangkou High, Huatung Basin, and Chimei Valley are steep about 6°-7° (Ramsey et al., 2006; Lallemand et al., 2013). The depth of the Chimei Valley is 3-4 km and relatively flat (Malavieille et al., 2002). The north of Chimei Valley is Takangkou High with the steep slope (Lehu., 2013). Besides, on the southern of the Chimei Valley is Changbin High that also has a steep slope (Lehu et al., 2015). Eastward from Chimei Valley is Huatung Basin which belongs to the abyssal zone (Lehu et al., 2016). Changbin and Takangkou High are composed of volcaniclastic deposits (Lallemand et al., 2016).

Hyperpycnal flow from the Xiuguluan River influences the mechanism of deposition on the eastern offshore of Taiwan (Lehu et al., 2015). Additionally, Kuroshio current induces longshore current throughout the eastern coast of Taiwan (Lehu et al., 2016). Longshore current is the ocean current that moves parallel with the coast (Ujiie et al., 2003). The marine sediment will be transported from south to north. Therefore, the possibility to deposit marine sediment from the shallow or deep marine on the onshore is very less (Jian et al., 2000). The mean of the Kuroshio current rate at 0-50 m in depth and 20-40 km in distance from the eastern coast is ~2.5 knots or 1.3 m/s (Hsin et al., 2008).

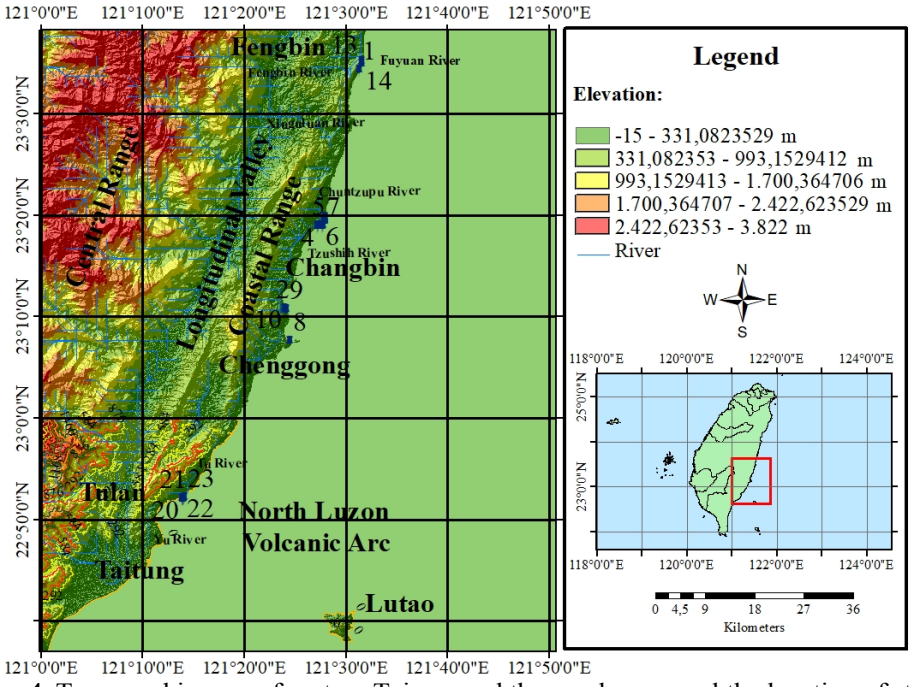

Figure 4. Topographic map of eastern Taiwan and the numbers reveal the location of stop sites

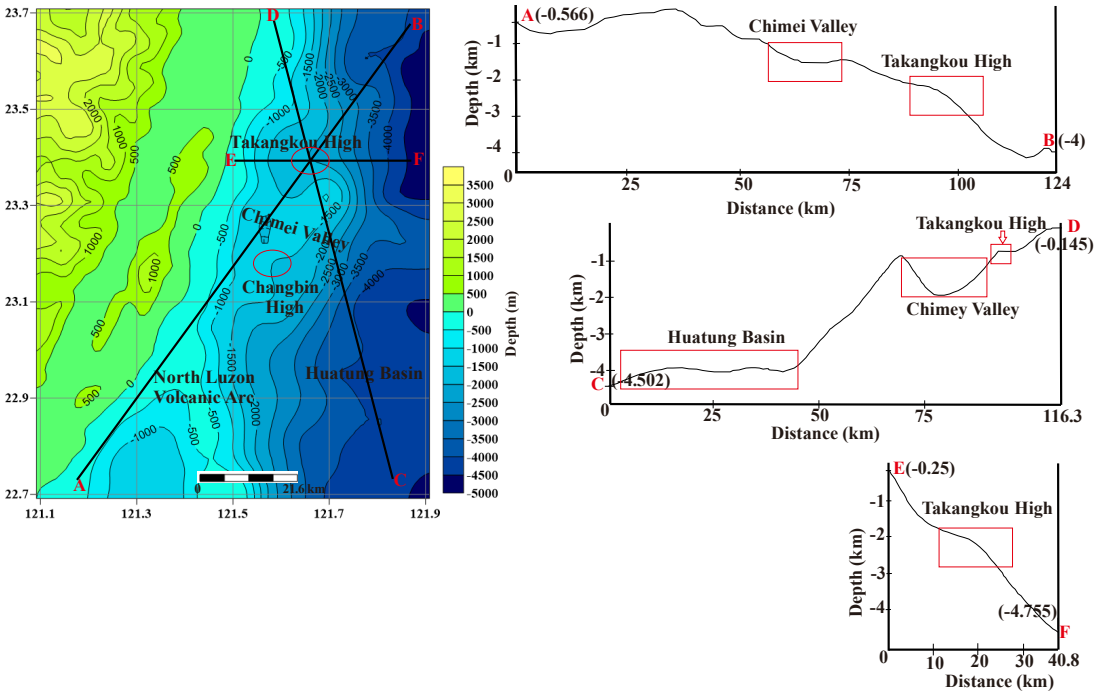

Figure 5. (A) Bathymetric map and (B) eastern Taiwan offshore bathymetric profiles. Isobaths every 500 m

Hyperpycnal flow occurs due to the density of the river water higher than basin water (Liew et al., 1990). Commonly, hyperpycnal flow takes place in the mouth of the river and formed during the flood (Ujiie et al., 2003). This flow moves and deposits sediment material in the gentle slope of the delta front and induce turbidite current (Lehu et al., 2015).

The depth of the Huatung Basin is approximately 4000 m. The characteristics of shoreline in eastern Taiwan are narrow coastal plain and terrace with less than 1 km in width. The ages of the terraces are younger than 20 ka. Huatung Basin consists of gravel transported by rivers draining in the Coastal Range. The composition is dominated by volcanic and metamorphic gravel. The origin of the metamorphic gravel is from Central Range with a low-grade metamorphism process. The difference between metamorphic and volcanic gravel is that metamorphic gravel has well-rounded sphericity owing to long-distance and duration of transportation. On the other hand, volcanic gravel has sub-angular to sub-rounded sphericity (Hsieh & Rau, 2009).

Taiwan is often hit by typhoons 3-4 times/year. The precipitation of rainfall can be as high as 2777 mm and has high landslide potential reaching 12,697 landslides (Ge et al., 2010) with a very high sedimentation rate. The high sedimentation rate in Taiwan are influenced by heavy rainfall, active tectonic activity, high frequency of typhoons, and high sediment supply from the river. Some rivers such as the Xiuguluan River, hyperpycnal flow has affected the sediment supply rate (Chen et al., 2004; Liu et al., 2008).

The drainage system in the eastern part of Taiwan from north to south consists of three large submarine canyons: Hualien, Chimei, and Taitung canyons (Lehu et al., 2015) (Fig. 1). The canyon as the deposition place of the sediment supply from the onshore. The sediment materials are derived from the Central and Coastal Ranges. The geological processes in the submarine are dominated by submarines erosional such as debris flow, submarine landslide, and turbidity currents (Ramsey et al., 2006). Throughout eastern offshore of Taiwan is passed by Kuroshio current that induces a longshore current. This current has an important role in suspended material transportation (Hsin et al., 2008).

Central Range and Coastal Range are separated by a Longitudinal Valley. Central Range is composed of metamorphic rock originated from continental margin whereas Coastal Range is dominated by volcanic formation (lava, pyroclastic, breccia, tuff) in the lower part which is related to island arc deformation (Miocene-early Pliocene). On the other hand, the upper part is the sedimentary sequence (muddy turbidite) generated at Fore-arc/Inter-arc basin. Sedimentary sequence is divided into 2 facies: volcanic and bio-clastic (Fanshuliao Formation) which are derived from a volcanic island and deep-sea conglomerate (Paliwan Formation) originated by material from Proto-Central Range like as quartzose grain and slate fragment (Hsieh et al., 2011).

The depth of the ocean basin (Huatung Basin) is approximately 4000 m. The characteristics of shoreline on eastern Taiwan are narrow coastal plain and terrace with less than 1 km in width. The ages of the terraces are younger than 20 ka. Huatung Basin consists of gravel transported by rivers draining in the Coastal Range. The composition is dominated by volcanic and metamorphic gravel. The origin of the metamorphic gravel is from Central Range with a low-grade metamorphism process. The difference between metamorphic and volcanic gravel is that metamorphic gravel has well-rounded sphericity owing to long-distance and duration of transportation. On the other hand, volcanic gravel has sub-angular to sub-rounded sphericity (Hsieh & Rau, 2009).

Figure 6 depicts seven rock formations in the study area. They are Pre-Neogene metamorphic complex, Tuluanshan Formation, Fanshuliao Formation, Lichi Formation, Paliwan Formation, Pleistocene conglomerate deposit, and floodplain, alluvial fan, terrace deposits (Wang et al., 1992; Chen & Wang, 1997).

Pre-Neogene Metamorphic Complex

The bedrock of eastern Taiwan is a pre-Neogene Metamorphic complex, reflecting the Asian continental crust. This complex compounds schist, marble, gneiss, and amphibolite which exist in the north.

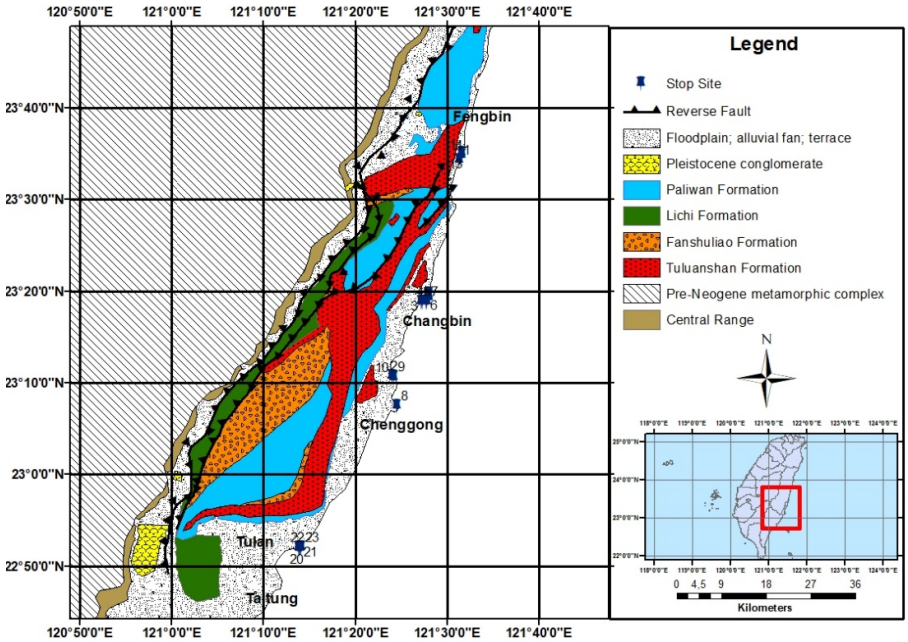

Figure 6. Geological map of eastern Taiwan displays rock formations and reverse fault along Fengbin to Tulan (after Wang *et al*., 1992; Chen and Wang, 1997). The downward sequence of rock formations in the legend reveals the age of them from youngest to the oldest

The schists comprise three types: green-schist, black schist, and siliceous schist which also consists of chert interlayers and quartz. These source rocks are various groups of shale, siltstone, sandstone, limestone, lava flow, and pyroclastic (Yen et al., 1951). The metamorphic grade of the rock is relatively low such as green-schist facies and amphibolite facies. The age of this metamorphic complex is Paleozoic to Mesozoic (Ho, 1986).

Pre-Neogene metamorphic complex is divided into two belts: the western Tailuko Belt and the eastern Yuli Belt. Both are distinguished by the dominant geological structure.

Tailuko Belt is characterized by open fold, meanwhile, Yuli's Belt is dominated by thrust fault (Yen, 1967). Allochthonous oceanic mafic and ultramafics are characterized by amphibolite bodies and serpentinite. in the northern part of Tailuko Belt is intruded by the late Mesozoic granitic rock which then changes the provenance of rock into gneiss (Ernst, 1983). Although this Tailuko Belt is dominated by low-grade metamorphic rocks, there are some high-grade metamorphic rocks such as felsic plutonic rock.

Yuli Belt includes a monotonous melange complex which is made up by oceanic pelitic schist containing a lot of mafic to ultramafic rocks (Jahn et al., 1981). Generally, the process of forming a Pre-Neogene metamorphic complex is divided into three episodes: 1) Formation of Yuli and Tailuko metamorphic Belts in the late Mesozoic (around 87 m.y.), 2) Recrystallization greenschist of Yuli and Tailuko metamorphic Belts in the late Miocene (8-14 m.y.), and 3) Collision of progressive metamorphism between the basement and the cover strata (< 4 m.y.) in Pliocene-Pleistocene (Chen et al., 1983; Lieu & Ernst, 1984).

Tuluanshan Formation

Tuluanshan Formation is composed of andesitic lava, tuff, pyroclastic breccia, and epiclastic conglomerate. Andesitic lava consists of sheet lava, breccia lava, and pillow lava which are dominated by hornblende and pyroxene minerals (Dorsey, 1992). Andesitic sheet lava is formed due to the spalling of the crust of lava during cooling contractions. Meanwhile, pillow lava is formed owing to the cooling of lava in the body of water. The characteristic of Tuff in this rock formation having fine to coarse grain grained ash beds, normal graded, and moderately-well sorted (Fisher & Schmincke, 1984). Tuff is generated from volcanic eruptions. pyroclastic breccia has the main mineral composition of pyroxene and hornblende, poorly sorted, and contains other components such as lapilli, coarse ash, and block clasts (Song & Lo, 1988). Pyroclastic breccia is derived from volcanic eruptions that catapult various volcanic materials and then move down the slope and deposited in the lower place. Fine volcanic materials would usually be suspended in the air and transported by the wind and will eventually be deposited in the depositional environment (Dolozi & Ayres, 1991). The epiclastic conglomerate has some characteristics such as well sorted, showing parallel/cross-lamination and grading structure. This deposit is generated by low/ high-density turbidity currents which may be derived from slumps in response to a combination of depositional seismic shocks and overstepping (Cole & Stanley, 1994). The age of this rock formation is approximately Miocene-Pliocene (Wang et al., 1992).

Fanshuliao Formation

This rock formation is composed of mudstone and sandstone. The distribution of this formation in the northern and western part of the Coastal Range along 180 km in length. In petrography, the quartzwacke sandstone and calcareous volcaniclastic sandstone (Teng, 1979; Dorsey, 1985; Chen, 1988). the quartzwacke constituent material is derived from the Eurasian continental plate exposed under the non-metamorphic proto-Taiwan sequence. This rock formation is a product of early Pliocene deposition (Wang et al., 1992).

Lichi Formation

Lichi melange Formation is a product of the Miocene subduction zone and the Pliocene-Pleistocene collision zone (Chen, 1988). The outcrop of this rock formation is spread over the eastern of the Longitudinal Valley. The typical characteristic of this rock formation outcrop is the elongate ellipsoidal blocks surrounding the foliated shally matrix. The block is dominated by sandstone with many joints, cracks, and web structures (Huang, 1969). Lichi Formation was deposited in Miocene-Pleistocene (Wang et al., 1992).

Paliwan Formation

Paliwan Formation consists of two members, Shuilien and Taiyuan members (Chen, 1988). Shuilien member is widespread in the northern Coastal Range and is dominated by conglomerate and sandstone. Taiyuan member is concentrated in the southern Coastal Range composed of sandstone/shale turbidite and mudstone. In petrography, Taiyuan member showing an abundance of quartz grain and rock fragments. The Bouma sequence of Taiyuan member reveals normal graded bedding with some other sedimentary structures like current ripple and parallel lamination (Teng, 1979). Essentially, Paliwan Formation is originated from deposition in the late Pliocene to early Pleistocene (Wang et al., 1992).

Pleistocene Conglomerate

Pleistocene conglomerate could be divided into two members. The first member is Shuilien conglomerate and the second is Peinanshan conglomerate (Chi et al., 1981). The uppermost of Shuilien conglomerate which has age around late Pliocene to early Pleistocene (3.60-1.68 Ma) is not covered by any deposit. On the other hand, the top of Chimei conglomerate is overlain by Takangkou Formation. The relative age of Chimei conglomerate roughly early Pleistocene (1.68-0.65 Ma) (Hsu, 1956). Basically, Shuilien conglomerate is deposited in the subaqueous fan delta system. Whereas, Chimei conglomerate is originated from deep-sea fan system (Dorsey, 1985).

Floodplain, Alluvial Fan, Terrace

Marine terrace deposit is divided into several facies. The succession of facies from old to young are offshore sand, nearshore sand, contorted marine sand, landslide/debris flow gravel, beach gravel, and fluvial gravel (Fig. 7) (Hsieh et al., 2011). Components of offshore sand facies are fine sand and silt.

This facies has horizontal/sub-horizontal laminated sedimentary structures that are possibly the product of storm deposit in nearshore-offshore. This facies is exposed only around Changbin. The nearshore sand facies are deposited in the shoreface environment and these outcrops can be found in the western part of Tulan Bay. This facies is composed of medium to coarse sand and contains abundant marine shell. The facies sedimentary structure is dominated by planar/trough cross-bedded and horizontal/sub-horizontal laminated (Nemec & Steel, 1984; Massari & Parea, 1988).

The upper part of nearshore sand facies is contorted marine sand. The constituents of this facies are mixing of sand with mud and containing significant marine shells, wood debris, and other marine fossils. The compositions of sand are rich in quartzose grains, meanwhile mud compositions consist of tuffaceous and non tuffaceous (Hsieh et al., 2011). This facies has less sedimentary structures. Basically, this facies has a more sedimentary structure, but the dewatering process caused the structure of sediment being damaged.

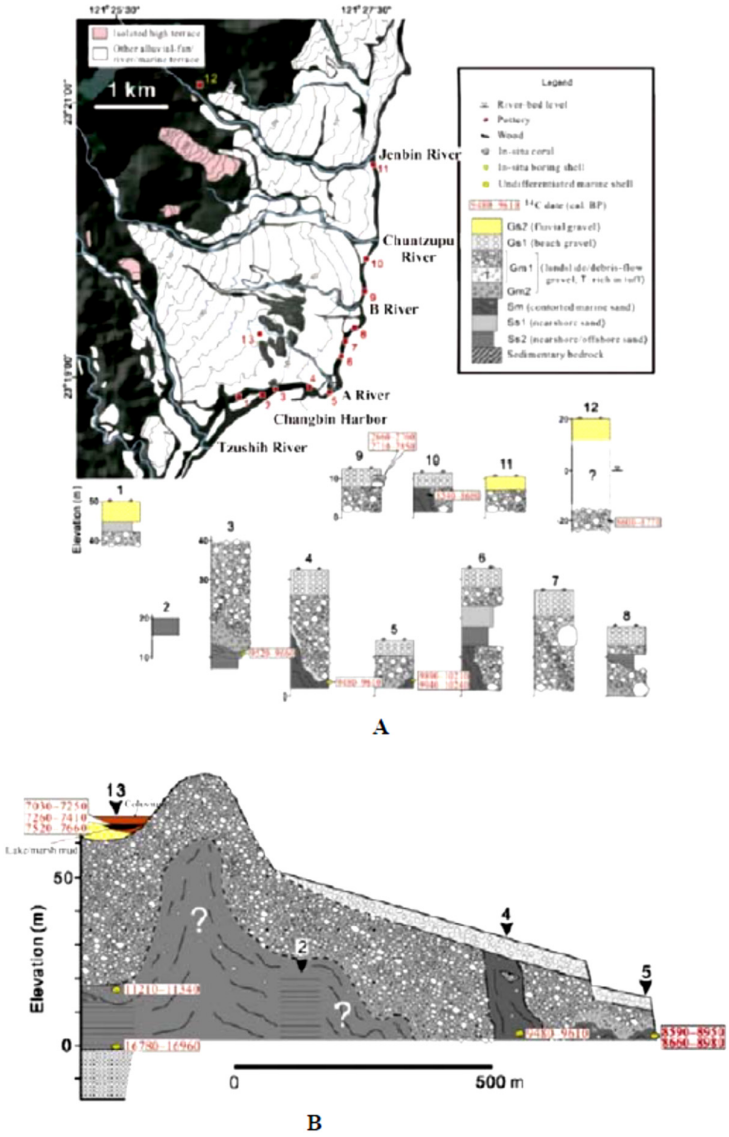

Figure 7. (A) Topography and stratigraphy of Changbin marine terrace. (B) Stratigraphic profile of Changbin marine terrace. Question marks in the stratigraphic profile illustrate the types of deposits are still questioned (Hsieh et al., 2011)

The dewatering process happened because of the factor of rapid sediment loading (Postma, 1983). This facies is identified as plastically deformed coastal/shallow marine deposits. The dispersion of such outcrops is in the eastern part of Tulan-Bay.

Landslide debris flows gravel is composed of angular/subangular volcanic gravel, metamorphic gravel, tuffaceous and non-tuffaceous matrix, wood debris, marine shell, and rounded metamorphic/volcanic gravel (Hsieh et al., 2011).

Moreover, many boulders are found resting on these deposits. The sedimentary features of this deposit are massive and matrix-supported. This facies was deposited in the submarine environment through mass-wasting processes (Hewitt, 2002). In the lower part of this deposit is dominated by a quartzose matrix and relatively containing finer grain size than the upper part. Based on the type of depositional, this deposit is the result of debris fall on Gilbert-type deltaic forests (Sohn et al., 1997). Likely, in the mechanism of deposition this facies, there is a mixing process between material derived from volcanic hillslope with coastal/ marine sediment. Materials derived from volcanic hillslope are transported through the river channel and then

when deposited are mixed with coastal/marine sediment.

Fluvial gravel deposit has constituent component characteristics such as subangular to subrounded volcanic gravel, many contain pottery fragments, and moderate to poor sorting. Basically, this facies is formed by fluvial depositional processes. The main sedimentary features contained in this facies are moderate to poorly stratified and clast-supported. On the other hand, beach gravel deposit is made up of rounded volcanic and metamorphic gravels (Hsieh et al., 2011). The sedimentary features of beach gravel facies are well-stratified, clast supported, and there is segregation of different grain sizes and shapes of clasts. Likely, the depositional environment of this facies is on the beach (Hunter, 1980).

Carbon Dating Data

Several previous studies undertook carbon dating on samples representing some deposits on the Changbin and Tulan marine terraces. Table 2 displays calibrated carbon dating data from many sources:

Earthquake and Tsunami Records

There were several earthquake and tsunami events in Taiwan particularly on the eastern coast of Taiwan (Hsieh & Rau, 2009). One of the huge earthquakes occurred in Taiwan is an earthquake that occurred on June 5, 1920. The magnitude of this earthquake was Mw 7.7 and induced a rupture on the southernmost Ryukyu trench (Theunissen et al., 2010). The precise position of the rupture is very close to Hualien. Another earthquake occurred on December 19, 1882, in Taitung with the magnitude of Mw 7.5. From 1771 until 2018, there were 30 earthquake events on the eastern coast of Taiwan with a moment magnitude scale (Mw) > 7. However, there was no record of the 1850 earthquake and tsunami as Ami's tribe folklore regarding a big sea wave in Chenggong. According to Ando et al. (2013), earthquakes and tsunami occurred in 1771 instead of 1850 as Ami’s folklore.

Table 2. Carbon dating data on the Changbin and Tulan marine terraces

Site	Calibrated Age (cal yr BP)	Material	Height (m)	Facies	Area	Source
3	9520-9660	Shell	11	DMS	Changbin	H1
6	9890-10,240	Shell	4	DMS	Changbin	L
15	2660-2850	Coral	8.5	BG	Changbin	C & H1
17	9200-9380	Shell	16	DMS	Tulan	H2
	9150-9330	Shell	4-10	DMS	Tulan	HS2
	16,750-16,910	Boring shell	0.5		Tulan	HS3
	2340-2490	Shell	23	BG	Tulan	H2
18	8420-8540	Wood	1	DMS	Tulan	HS1
19	12,610-12,850	Shell	6.5	BSB	Tulan	HS2
	13,970-14,210	Shell	5	BSB	Tulan	HS2
	12,760-13,080	Shell	7	BSB	Tulan	Y
	16,650-16,840	Boring shell	2.5		Tulan	HS3
20	8800-9000	Shell	5	DMS	Tulan	H2
	9080-9240	Shell	5-8	DMS	Tulan	HS2
21	8420-8540	Wood	1	AVL	Tulan	C
	8660-8980	Wood	3	AVU	Tulan	HS3
26	8540-8680	Wood	6	DMS	Changbin	HS1
30	9480-9610	Shell	4	DMS	Changbin	H1

[a] Referred to Fig. 2, 4, 6, and 7.

[b] DMS = Deep marine sand; BG = Beach gravel; BSB = Beach sand bottom; AVL = Alluvial fan lower part; AVU = Alluvial fan upper part. H1 = Hsu et al. (1998); H2 = Hsu et al. (1999); L = Liew et al. (1993); HS1 = Hsieh (1990); HS2 = Hsieh et al. (2004); HS3 = Hsieh et al. (2011); Y = Yamaguchi and Ota, (2004); C = Chen et al. (1991).

The height of the sea wave reached five meters and hit Ami's tribe settlement in Chenggong. Another possibility, it's the event is a storm. However, storm wave run-up occurred worldwide never reach five meters. Moreover, based on Zhou & Adams (1985); Ma & Lee (1997); Hsieh & Rau (2009); Lau et al., (2010), the height of tsunami waves on the eastern coast of Taiwan had never reached 1 m. Most tsunami events only occurred in offshore. Earthquake and tsunami records in Taiwan can be seen in Table 3:

Table 3. Earthquake and tsunami records in Taiwan from 1771-2018

Years	Moment Magnitude (Mw)	Location	Explanation and Reference
1771	>7	Chenggong	Earthquake and tsunami (Ando et al., 2018)
1781	>7	Tainan	Earthquake and moderate tsunami (Lau et al., 2010)
1782	>7	Tainan	Earthquake and moderate tsunami (Lau et al., 2010)
1811	7.5	Hualien	Earthquake (Tsai, 1985)
1815	7.7	Hualien	Earthquake (Tsai, 1985)
1867	>7	Keelung	Earthquake and moderate tsunami (Zhou &Adams, 1985; Lau et al., 2010)
1882	7.5	Taitung	Earthquake (Tsai, 1985)
1917	>7	Eastern coast of Taiwan	Earthquake and moderate tsunami (Ma & Lee, 1997; Lau et al., 2010)
1920	7.7	Hualien	Earthquake (Theunissen et al., 2010)
1922	7.6	Eastern coast of Taiwan	Earthquake and moderate tsunami (Ma & Lee, 1997; Lau et al., 2010)
1951	>7	Eastern coast of Taiwan	Earthquake and moderate tsunami (Ma & Lee, 1997; Lau et al., 2010)
1960	>7	Eastern coast of Taiwan	Earthquake and moderate tsunami (Ma & Lee, 1997; Lau et al., 2010)
1963	7.3	Northeastern coast of Taiwan	Earthquake and moderate tsunami (Ma & Lee, 1997; Lau et al., 2010)
1964	>7	Eastern coast of Taiwan	Earthquake and moderate tsunami (Ma & Lee, 1997; Lau et al., 2010)
1966	7.6	Northeastern coast of Taiwan	Earthquake and moderate tsunami (Ma & Lee, 1997; Lau et al., 2010)
1972	>7	Eastern coast of Taiwan	Earthquake and moderate tsunami (Ma & Lee, 1997; Lau et al., 2010)
1978	>7	Eastern coast of Taiwan	Earthquake and moderate tsunami (Ma & Lee, 1997; Lau et al., 2010)
1986	>7	Eastern coast of Taiwan	Earthquake and moderate tsunami (Ma & Lee, 1997; Lau et al., 2010)
1993	>7	Eastern coast of Taiwan	Earthquake and moderate tsunami (Ma & Lee, 1997; Lau et al., 2010)
1996	>7	Eastern coast of Taiwan	Earthquake and moderate tsunami (Ma & Lee, 1997; Lau et al., 2010)
1998	>7	Eastern coast of Taiwan	Earthquake and moderate tsunami (Ma & Lee, 1997; Lau et al., 2010)
1999	>7	Eastern coast of Taiwan	Earthquake and moderate tsunami (Ma & Lee, 1997; Lau et al., 2010)
2001	>7	Eastern coast of Taiwan	Earthquake and moderate tsunami (Ma & Lee, 1997; Lau et al., 2010)
2002	>7	Eastern coast of Taiwan	Earthquake and moderate tsunami (Ma & Lee, 1997; Lau et al., 2010)
2003	6.8	Chenggong	Earthquake (Hsieh & Rau, 2009)
2004	5.8	Hualien	Earthquake
2009	6.4	Hualien	Earthquake
2013	6.3	Hualien	Earthquake
2015	6.3	Hualien	Earthquake
2018	6.4	Hualien	Earthquake

Holocene Sea-Level Changes

Post-glacial sea-level data (0-10 ka) refers to the sea-level change curve according to Chen and Liu (1996, 2000). They undertook carbon dating at the coral platform and coarse-grained detrital mollusk shells in Penghu Island, west of Taiwan. Penghu Island was picked as the location for knowing the Holocene sea-level change in Taiwan because it is considered to have relatively stable tectonic activity (Chen & Liu, 1996). Figure 8 depicts that sea-level at 3-5 ka is +2 ± 1 m, 6 and 10 ka is -30 ± 7 m. The average sea-level rise rate for 10-6 ka is 7 mm /yr to 10 mm / yr (Chen & Liu 1996, 2000). The highest sea-level rise is 2.4 m above the modern sea-level happened 4700 years ago (Chen & Liu, 1996). Afterward, the sea-level down to the present position without large fluctuations (Hsieh et al., 2004).

Methodology

Field Observation

There are five types of samples collected in the Fengbin area. The coordinate location of the sampling is on the stop site 1(La: 121.5216917; Lo: 23.570675, 13 (La: 121.5260444; Lo: 23.58459444), and 14 (La: 121.5252639; Lo: 23.580475). The first samples are sedimentary rocks obtained on the marine terrace outcrop in Fengbin (Fig. 9A). Rock sampling represents each rock layer on several sampling sites. The second samples are sedimentary rocks found on the outcrop located on the river edge approximately 100 meters from the shoreline (Fig. 9D) The third samples are loose sediment (unconsolidated material) taken from the marine terrace (Fig. 9E). While the fourth and fifth samples are unconsolidated materials from the outcrop on the river edge (Fig. 9B). Modern beach sand is also collected (Fig. 9C). The diameter of the consolidated material is 30-40 mm. Meanwhile, the sample size for unconsolidated materials has a weight of roughly 200-500 grams.

Point Counting Analysis

The sand counting method is used in this study to differentiate beach sand and fluvial sand. Therefore, the Gazzi-Dickinson technique is adopted to calculate the percentage of sandstone components. It begins by making several thin sections of the rock representing each target layer in several sampling sites. Beach sands are collected from two different sites in Fengbin. Fluvial sand samples are taken from two sites in Fengbin.

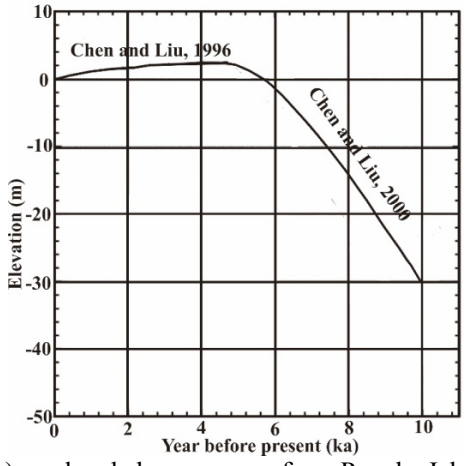

Figure 8. Post-glacial (0-10 ka) sea-level change curve from Penghu Island (Chen and Liu, 1996; 2000)

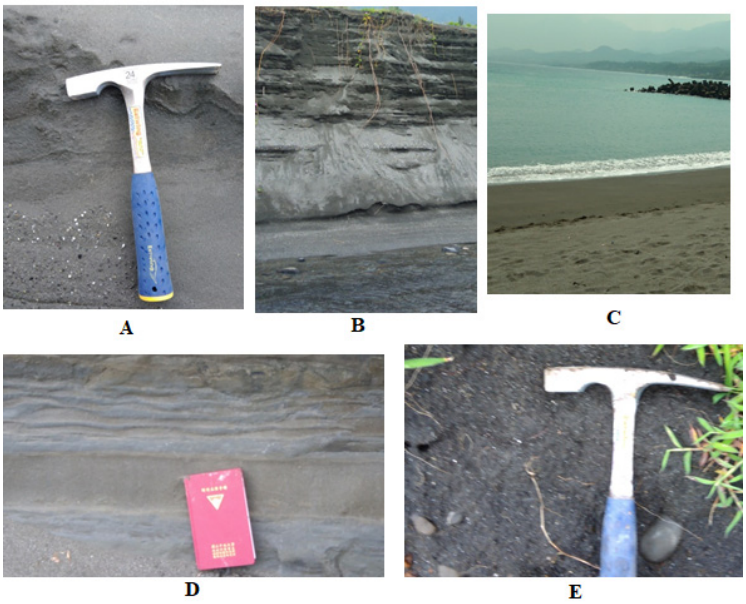

Figure 9. The kind of samples collected from the field. (A) consolidated materials on the marine terrace, (B) loose sediments on the bank of the river, (C) modern beach sand, (D) consolidated materials from the outcrop on the bank of the river, (E) unconsolidated materials from the marine terrace

Three important components that are calculated in this method is the percentage of rock fragment, quartz, and feldspar. We must be able to distinguish among lithic of volcanic, metamorphic, and sediment. After completing the calculation of the components, the next step is plotting their percentage in the sand counting triangle. Eventually, we can know the different components of them and interpret the provenance, genesis, and rock facies. We use microscope photograph software to take a photo of minerals. Two software packages that are used to help analysis in this method, namely Image Fiji and Grapher 12. Image Fiji is a tool to calculate the percentage of quartz, feldspar, and rock fragment on thin-section photos. Meanwhile, Grapher 12 is applied to make the sand counting triangle.

Biozonation

In biozonation analysis (Table 12), we used planktonic foraminifera fossils. The use of this fossil because planktonic foraminifera has a short lifespan so that the relative age range is not too long. In addition, foraminifera is one kind of index fossil that could be used to determine the relative age of a rock layer. Moreover, planktonic foraminifera has large abundance, easily identifiable, and spread widely. The interval and assemblage zones are used in determining the relative age of sediment deposits. The first occurence (FO) of the taxon identifier is the main principle of interval zone. Meanwhile, zone assemblage is carried out by using one or more fossil species of planktonic foraminifera which have the same age. There are five samples with a thickness of each sample is 9 cm. So that the total thickness reaches 45 cm. We identify the species name and the abundance of each species in each sample. Then, we determine the relative age of the species found based on Postuma (1971). After being correlated with Postuma (1971), it is possible to divide the biostratigraphic zones by applying the principles of assemblage and interval zones. This biostratigraphic zone reflects the relative age of the rocks.

Paleo-bathymetry

The paleo-bathymetry analysis is adopted to examine the depositional environment. In this

analysis, we identify benthic foraminifera and describe their living environment. The determination of the depositional environment is based on the distribution and abundance of benthic foraminifera fossils that live at a certain depth or based on assemblage zone. Benthic foraminifera environment is crucial for determining the type of extreme flood events, i.e. tsunami or storms. the existence of benthic foraminifera can be associated with big sea waves that transport them from marine into transitional environments. Nevertheless, in some cases, the existence of foraminifera can be attributed to the change in sea water level. Nonetheless in this study area since Holocene, the maximum sea-level rise is 2.4 m above the modern sea-level. It occurred in 4.7 ka. The percent ratio technique between the number of planktonic foraminifera with the total addition of planktonic and benthic foraminifera (Table 4) used to strengthen the identification of fossil and sedimentary origin. The percent ratio is classified into a depositional environment according to Grimsdale and Markoven (Wijaya et al., 2017). The most important consideration in this research is the marine terrace on the eastern coast of Taiwan rapidly uplift.

Granulometric

The granulometric analysis used in this study is a graphical technique. The principle of this technique is to plot the result of grain fraction sieving and weighing as cumulative curves to find out the statistical parameters. Prior to the samples being sieved, all sieves should be cleaned by a brush. Each sample is undertaken as the first measurement of weight. Afterward, arrange the sieve in succession from the biggest mesh number on the bottom to the smallest number on the top. We adopt the bottom pan at the lowest part. The samples were poured into the sieve and cover the top then and the wait for 5 to 15 minutes of shaking.

Sorting of the grain fraction is carried out from the top to the bottom pan. Picking is done by pouring granules in each shaking sieve with a soft brush. Weight loss should not be greater than 5%. Furthermore, we measure the weight of each fraction and stored in the sample bag that has been given a mesh number according to the sieve number. Furthermore, the results are presented in a table. Subsequently, the cumulative curve can be made by using semilog paper. the cumulative curve can determine the statistical parameters that needed. The result of calculations is incorporated into the existing formula to find out Md, So, Sk, and K values. Meanwhile, in the mathematical method, we adopt several mathematic equations to get Md, So, Sk, and K.

Results and Discussion

The AV deposit (Fig. 10) in this location tends to have characteristics grayish-brown color and consisting of disorganized mixtures such as containing sand materials, sub-angular to very angular volcanic and metamorphic gravels, pebbles, cobbles, and boulders. The thickness of this deposit is more than one meter. This deposit includes a grain supported type which means that coarse materials such as gravel, pebble, cobble, even boulder are more dominant than sand materials. Volcanic fragments are constituted by pyroxene, quartz, plagioclase feldspar, and hornblende. Meanwhile, metamorphic fragments indicating an abundance of low-grade metamorphic provenance such as (green schists, glaucophane schist, phyllites, and slate fragments) that likely derived from a pre-Neogene metamorphic complex in the Central Range and deposited by mass-wasting processes. The low-grade metamorphism rock can be identified by mineral association consisting of albite, muscovite, and chlorite.

Mass wasting processes are interpreted by the transport of sediments originating from the Coastal Range by the Fengbin and Fuyuan Rivers. The distance of transportation from the provenance to the depositional environment is relatively close. In addition, the transportation time is comparatively short.

Table 4. classification of the relationship between the percent of planktonic and benthic foraminifera ratios with the depositional environment according to Grimsdale and Markoven (Wijaya et al., 2017)

No	%P/B	Depth (m)	Depositional Environment
1	0-20	0-20	Inner shelf
2	20-30	20-100	Middle shelf
3	30-50	100-200	Outer shelf
4	50-80	200-1000	Upper shelf
5	80-100	1000-4000	Lower shelf

$$\%P/B = \frac{P}{(P+B)}.100\% \quad \text{.....(1)}$$

Where:
P = the amount of planktonic foraminifera
B = the amount of benthic foraminifera

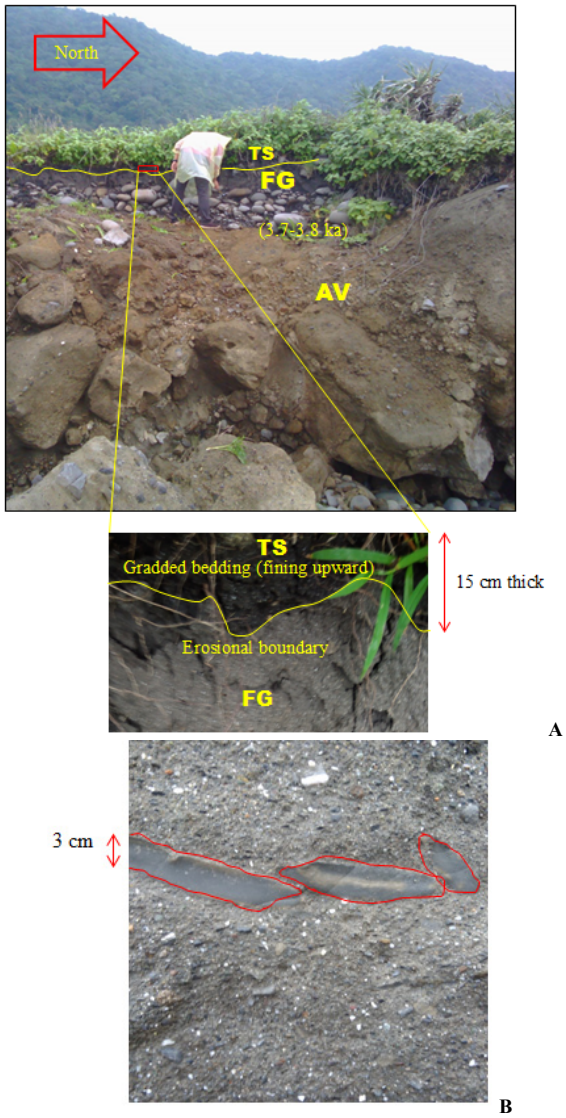

Figure 10. (A) Photos of a marine terrace at SS-1 in Fengbin. This outcrop consists of the AV, FG, and TS deposits. On the upper part of FG layer, there is about 15 cm thickness of TS at 11.5 m in altitude. Erosional boundary separates between FG and TS. They depict graded bedding structure. The uppermost part is trapped by soil. The distance of the outcrop to the shoreline roughly 50 m. (B) Rip-up clasts structure in TS deposit at SS-1

The level of transportation energy is considered as low-energy in contrast with depositional energy which can be classified as a high-energy deposition. This interpretation is based on the sphericity of components having sub-angular to very angular and grain size containing a lot of coarse materials. These indicate that the processes of erosion during transportation are not intensive. The intensity of erosion depends on several factors like time of erosion, the distance of provenance to the depositional environment, and transportation energy. Based on deposit characteristics and depositional mechanisms, the AV deposit is called an alluvial fan. It is also in accordance with the interpretation of Hsieh et al. (2011).

The upper part of the alluvial fan deposit is FG (Fig. 10). It seems grayish and consists of the sub-rounded to rounded volcanic gravels. This deposit also contains coarse to very coarse sands. Moreover, it has the main characteristics of gray, poor extended, and discontinuous bedding. There are two distinct features in this deposit. The lower part makes up most of the gravel to cobble-sized, whereas the upper part is dominated coarse to very coarse sands. Sand blow structure is present in this upper part. This structure is an indicator of the occurrence of earthquake events that caused the liquefaction. The pressure caused by an earthquake can push sand and groundwater to the surface. It's characteristics are comparable with the gravel deposits along the Fengbin and Fuyuan rivers. They can be classified as grain supported with poorly sorted. The sand components do not exhibit a positive reaction to the HCl solution. Therefore, they can be assumed as non-carbonate sands. Organism components that are discovered encompass terrestrial shells, wood and plant debris. Therefore, an FG deposit can be interpreted as fluvial gravel. This interpretation is similar to the opinion of Hsieh *et al*. (2011). The thickness of this deposit is approximately one meter. There is no information about the age of these deposits. However, if we refer to the carbon dating data of the fluvial gravel deposit in Hsinshe, the age of these deposits can be estimated at about 3.7-3.8 ka (Hsieh, 2004). Fluvial gravel deposits in Hsinshe and Fengbin reveal the same characteristics and their distance is not far from each other only 5 km. This facies is deposited notably by fluvial processes.

Fluvial gravel is overlain by TS (Fig. 10). It contains volcanic fragments, lithic of sediments, quartzose grains, coral fragments, shell fragments, wood, and plant debris. It has a positive reaction to the HCl solution. This implies as carbonate sand. TS deposit identical to modern beach sand. The thickness of this facies is around 15 cm. This deposit is considered as an extreme flood event product. The color of this deposit seems darker than the fluvial gravel deposit in the lower part. Both deposits are separated by an erosional boundary. Rip-up clasts, planar lamination, cross-bedding, scour and fill structures were discovered in this deposit. Based on the granulometric analysis (Table 5 and 6), TS deposit is dominated by medium and coarse sands (75.726% of the total component of sands). The result of the granulometric analysis indicates moderately sorted (So = 0.7505), strongly fine skewed (Sk = 0.58198), and very lepto kurtic (K = 2.7495) (Folk & Ward, 1957).

Sorting, skewness, and kurtosis are obtained from equation 1, 2, and 3:

$$So = \sqrt{\frac{\sum f.(m\phi - x)^2}{100}} \quad \text{.....} \qquad \text{.....(1)}$$

$$Sk = \sqrt{\frac{\sum f.(m\phi - x)^3}{100.So^3}} \quad \text{.....} \qquad \text{..(2)}$$

$$K = \frac{\sum f.(m\phi - x)^4}{100.So^4} \quad \text{.....} \qquad \text{... ...(3)}$$

Where:
So = sorting

f = frequency
m Φ = mid point of diameter phi
x = mΦ/10
Sk = Skewness
K = kurtic

Therefore, this layer is likely deposited in medium to high transportation energy and low to medium deposition energy with some distance away from the provenance. Moreover, grain components have moderate to strong resistance. Generally, sorting reflects depositional energy, the distance of transportation from provenances to the depositional environment, and rock resistance to erosion. Positive skewness indicates that the sediment has a high number of coarse grains compared to the number of fine grains. Kurtosis shows the comparison between the middle segmentation to the edge of a curve.

Grain size distribution depicts the unimodal curve and predominantly medium sand (Fig. 11). The gradient of the curve seems steep and increases gradually which means the provenance derived from the single source and transported by saltation mechanism. There are no specific criteria for the sorting, skewness, and kurtosis values to discriminate tsunami and storm deposits. Putra (2018) states tsunami and storm studies that have been conducted in various places indicate the variation of sorting from well-sorted to poorly sorted.

Table 5. The grain classification of TS deposit is dominated by medium and coarse sands

Site	Grain Classification	Diameter (mm)	Diameter Phi (Φ)	Mid point (Mθ)	Frequency (gr)	Frequency (%)	Cumulative (%)
SS-1		0.0625	4				
SS-1	Very fine sand			3.5	8.7	2.74257613	2.74257613
SS-1		0.125	3				
SS-1	Fine sand			2.5	68.3	21.53079881	24.27337494
SS-1		0.25	2				
SS-1	Medium sand			1.5	164.33	51.803165	76.07653994
SS-1		0.5	1				
SS-1	Coarse sand			0.5	75.89	23.92346006	100
		1	0				
Total					317.22	100	

Table 6. the classification of sorting, skewness, and kurtosis indicate moderately sorted, strongly fine skewed, and very lepto kurtic

Mθ.f	(Mθ-x)	$(Mθ-x)^2$	$f.(Mθ-x)^2$	$(Mθ-x)^3$	$f.(Mθ-x)^3$	$(Mθ-x)^4$	$f.(Mθ-x)^4$
9.599016455	1.96907509	3.877256709	10.6336717	7.634609603	20.93849806	15.03311959	41.22947495
53.82699704	0.96907509	0.93910653	20.21971376	0.910064745	19.59442093	0.881921074	18.98846522
77.70474749	-0.03092491	0.00095635	0.04954196	-2.9575E-05	-0.001532081	9.14605E-07	4.73795E-05
11.96173003	-1.03092491	1.06280617	25.42600097	-1.095673356	-26.21229776	1.129556956	27.02291072
Total							
153.092491		Total	56.32892839	Total	14.31908914	Total	87.24089827
1.53092491		Total/10	0.563289284	Total/10	0.143190891	Total/10	0.872408983
Sorting	0.750526005	0.422763256	0.317294817				
		42.27632558	31.72948173				
Skewness	0.581981366						
Kurtosis	2.749521691						

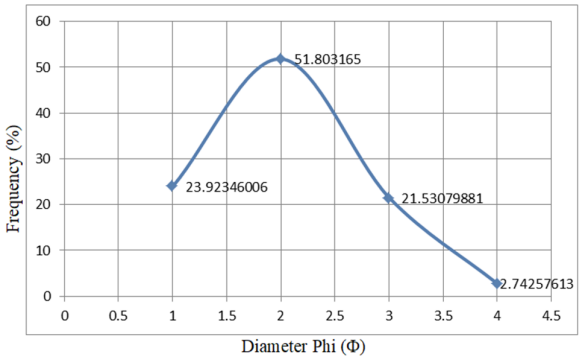

Figure 11. Grain size distribution curve on TS deposit at SS-1. The curve denotes unimodal owing to it has one culmination

The sorting value is related to the source of sediment. If a deposit has a poorly sorted characteristic then it can be deduced that the origin of the sediment has highly grain size variation. Grain size distribution curve shapes such as unimodal and bimodal are associated with the type of sediment origin, tsunami transport, and depositional process. The variations in grain size and bimodal distribution curves are the most common characteristics of tsunami sediments such as the 1993 tsunami deposition in Hokkaido-Nansei-Oki, the 2004 tsunami in the southern Andaman Islands of India, and the 1960 tsunami in Chile. This happens because there are two phases of the tsunami wave with different transportation energy. The first phase is a run-up wave that has large transport energy and carries marine and beach sediments. The second phase is the backwash where the waves return to the sea with terrestrial and beach sediments. All of these processes are rapid and the granulometric result is characterized by two peaks grain size distribution curves (bimodal) (Fujiwara, 2008; Sarkar et al., 2013; Putra, 2018). They cannot be a single indicator to differentiate tsunami and storm deposits. Meanwhile, the thickness variation of tsunami deposits in various places is controlled by local topography. Therefore, a tsunami event will yield a different thickness of the deposit between one place with other places. However, the tsunami deposit has particular characteristics like fining upward and thinning inland (Morton et al., 2007).

In contrast to tsunamis and storm deposits that have various sorting characteristics, the sand deposits formed during the transgression period tend to be dominant well-sorted to very well sorted. This is influenced by the relatively slow settling time, so that the sediment material will experience intensive erosion. Intensive erosion will cause grain size diversity to decrease (Folk & Ward, 1957).

Two samples of modern beach sand and TS sand are conducted in the petrographic analysis. The result exhibits predominantly polycrystalline quartz minerals and lithic of sedimentary rocks (Fig. 12). Other components are volcanic rock fragment and monocrystalline quartz. Polycrystalline quartz is a mineral that is often found in metamorphic rocks. Tsunami sediment is a mixture of marine and beach sediments. Marine sediments are transported by tsunami waves during the run-up. Meanwhile, beach and terrestrial sediments are transported during the backwash. Coastal and terrestrial sediments on Taiwan's east coast are dominated by material originating from the pre-Neogene metamorphic complex in Taiwan's central range. The material is transported and deposited on the east coast through the Xiuguluan, Fuyuan, and Fengbin rivers. Pre-Neogene metamorphic complexes in the central range of Taiwan are dominated by silica minerals, especially monocrystalline and polycrystalline quartz (Yu et al., 2015). In addition, there is a possibility that this fragment is derived from the metamorphic rock component formed in the Ryukyu Trench zone. The same characteristics were found in tsunami deposits on Ishigaki Island, Japan. Fragments of metamorphic rock components, mainly polycrystalline quartz, dominate tsunami deposits on Ishigaki Island (Ando et al., 2018).

The process of erosion induces the metamorphic rock components to break apart into fragments of various sizes. A high energy flow regime carries such materials to nearshore then accumulated and deposited. Lithic of sedimentary rock shows a mixture of reworking materials derived from offshore with components derived from onshore. Whereas, the characteristic of volcanic rock fragment and monocrystalline quartz shows similarity with the result of petrographic analysis of andesitic rock of Tuluanshan Formation (Chen & Wang, 1997). It can be deduced that volcanic rock fragments and monocrystalline quartz are derived from Coastal Range.

Modern beach sand and TS sand contain marine organisms such as benthic and planktonic foraminifera. Benthic foraminifera species found in both deposits at SS-1 are *Elphidium craticulatum* (Fig. 13C), *Rotalinoides compressiuscula*, and *Quinqueloculina auberiana*. Commonly, they live in a shallow marine with 100-200 m in depth. Planktonic foraminifera is contained in the tsunami deposit at SS-1 are *Neogloboquadrina incompta* (Fig. 13A), *Orbulina universa* (Fig. 13B) and *Trilobatus sacculifer*. They exist from Miocene to Quaternary Period. Mollusca (Gastropoda), echinoids (shells), and coral fragments also present in this deposit. Besides, terrestrial organisms are also discovered in both, which are terrestrial shells, wood, and plant debris.

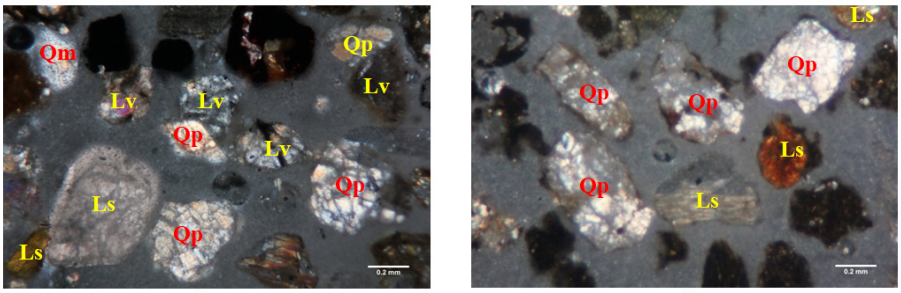

Figure 12. (A) Thin section of modern beach sand and (B) TS sand. They have similar compositions such as polycrystalline quartz (Qp), monocrystalline quartz (Qm), and sedimentary rock fragment (Ls). Both distinction are modern beach sand contains volcanic fragment (Lv) but TS sand does not comprise it

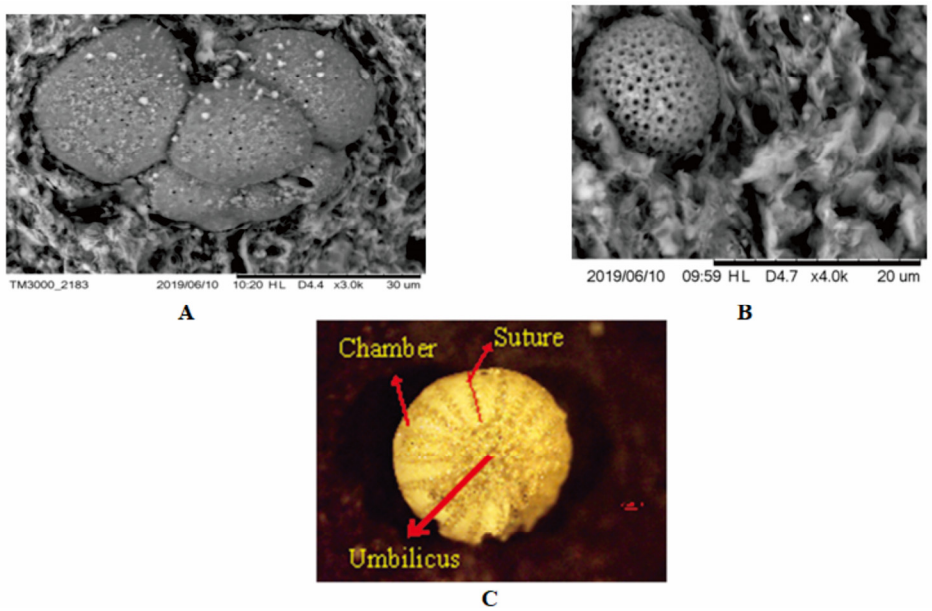

Figure 13. planktonic foraminifera (A) *Neogloboquadrina incompta* and (B) *Orbulina universa*. (C) benthic foraminifera *Elphidium craticulatum*

Deposits from old to young at SS-13 (Fig. 14) and SS-14 (Fig. 14) are AV, FG, and TS deposits. Soil covers TS sand in the upper part. The characteristic of deposits found at SS-13 and SS-14 are the same as the previous site. This can be inferred that the source of sediment material, transport mechanisms, and deposition process are identical. The height of outcrops at SS-13 and SS-14 is 11 m and 13 m. The AV deposit components are composed of pebbles and cobbles volcanic rock breccia, volcanic and metamorphic gravels, and tuffaceous matrix. Wood debris also presents in this deposit. The bedding of this deposit is very steep may originate from debris fall. Therefore, AV is interpreted as an alluvial fan. This interpretation appropriate with the hypothesis proposed by Hsieh et al. (2011). The thickness of the alluvial fan is more than one meter. An alluvial fan is covered by FG deposits which have the same characteristics as the previous site. The grain size of these deposits varies greatly. At the lower part, it is dominated by volcanic gravel to cobble. Meanwhile, the upper part is predominantly coarse sand to very coarse sand. The lower part and upper part of FG deposits are still classified as one facies. Sand deposits do not react positively to the HCl solution. Therefore, such a deposit includes non-carbonate sand. The thickness of these deposits is more than one meter. The vertical distribution pattern depicts fining upward. Additionally, these deposits seem poor extended and discontinuous bedding. The characteristic is similar to fluvial deposits in Fengbin and Fuyuan Rivers. Therefore, these deposits may be originated from the transported material of both rivers. These deposits are interpreted as fluvial gravel.

Fluvial gravel deposits are overlain by TS deposits. The thickness of the TS deposit at SS-13 and SS-14 is 20 cm and 15 cm (Fig. 15). The color of the TS deposit at SS-13 seems brighter than SS-1. This is due to the intensity of weathering at SS-1 more intensive than SS-13. Erosional boundary becomes the boundary between FG and TS deposits.

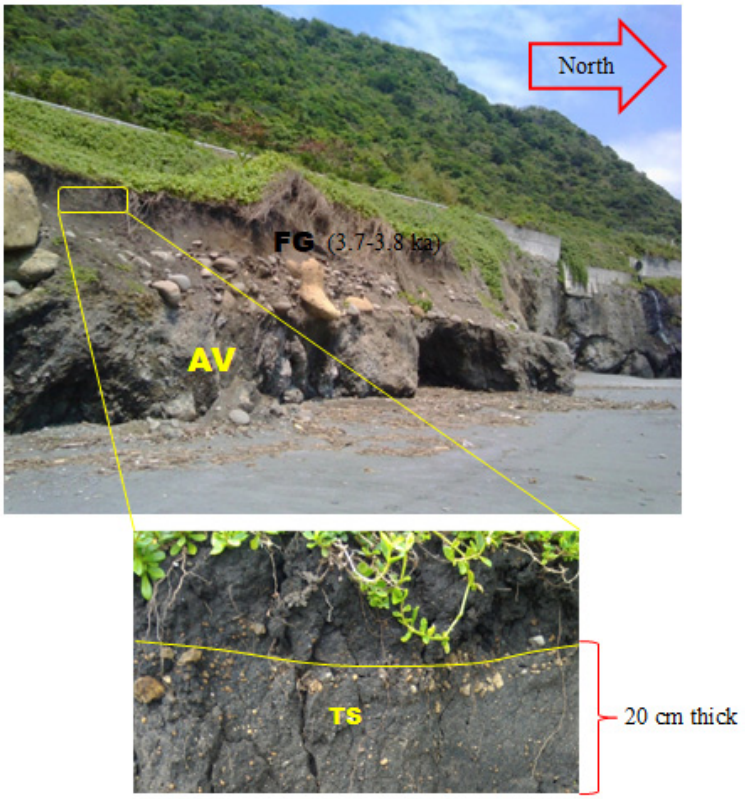

Figure 14. Photo of a marine terrace at SS-13 in Fengbin. The sequence of sediments from oldest to youngest is AV, FG, and TS deposits. The thickness of TS deposit is around 20 cm. It contains materials from terrestrial and marine deposits

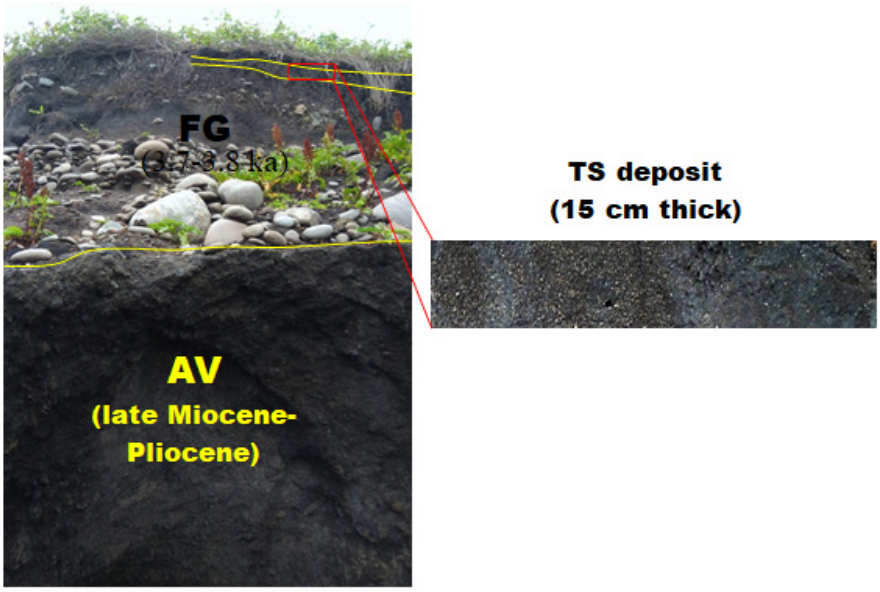

Figure 15. Marine terrace outcrop at SS-14 in Fengbin. This outcrop is composed by AV, FG, and 15 cm TS deposit thick. The age of AV deposit is around late Miocene to Pliocene. Whereas the age of FG deposit is 3.7 to 3.8 ka (Hsieh, 2004)

When a high flow regime occurred, the transport energy of the wave erodes the previous deposit. Besides, the high flow regime also precipitates sedimentary material from the marine zone toward terrestrial. Generally, when a high flow regime comes to the onshore, they carry marine sedimentary materials by traction, saltation, and suspension transport mechanisms.

Meanwhile, when backwash, transport energy decreases and vice versa the deposition energy increases. A high flow regime will precipitate sediment material from terrestrial. Thus, there is an accumulation of sediments from terrestrial and marine.

The result of the petrographic analysis shows that compositions of TS sand at SS-13 (Fig. 16 A) and SS-14 (Fig. 16 B) are comparable with modern beach sand at SS-13 and SS-14 (Fig. 16 C and D). They are dominated by polycrystalline quartz and sedimentary rock fragments. These components are the same as TS sand at SS-1. Fluvial sand samples in outcrops (Fig. 16 E) and modern fluvial sand (Fig. 16 F) from Fengbin River around SS-13 and SS-14 were collected to discriminate between TS deposit and other deposits.

Table 7 shows the grain size distribution of TS deposits at SS-13, and none of which dominates absolutely. The percentage frequency of fine sand, coarse sand, and the sand medium is almost the same. It is indicated that grain size is evenly distributed. The sorting value indicates very poorly sorted which means varied grain size distribution. It can be interpreted that the source of sediment materials has a variety of grain sizes. Skewness value is classified near symmetrical which means the percentage of fine grain and coarse grain is almost the same. Kurtosis is categorized as very platykurtic (Table 8) (Folk & Ward, 1957).

TS deposit grain size distribution curve at SS-13 (Fig. 17) moves down gradually at the beginning, then moves up until reaching the peak point. Subsequently, the curve moves down gradually. These can be interpreted beginning from the traction transport mechanism saltation transport mechanism. The curve shape denotes unimodal because it has one culmination. This indicates a single source material.

The result of granulometry analysis is illustrated in table 9 and figure 18. The highest percentage of grain size classification is medium sand although the difference of percentage frequency with others is not significant. Granulometric analysis of TS deposit at SS-14 displays similar results with SS-13.

Table 7. The grain size distribution of the TS deposits at SS-13 is almost same. This is representated by the same frequency percentage

Site	Grain Classification	Diameter (mm)	Diameter Phi (Φ)	Mid point (Mθ)	Frequency (gr)	Frequency (%)	Cumulative (%)
SS-1		0.0625	4				
SS-1	Very fine sand			3.5	43.49	10.98232323	10.98232323
SS-1		0.125	3				
SS-1	Fine sand			2.5	151.14	38.16666667	49.1489899
SS-1		0.25	2				
SS-1	Medium sand			1.5	79.44	20.06060606	69.20959596
SS-1		0.5	1				
SS-1	Coarse sand			0.5	121.93	30.79040404	100
		1	0				
Total					396	100	

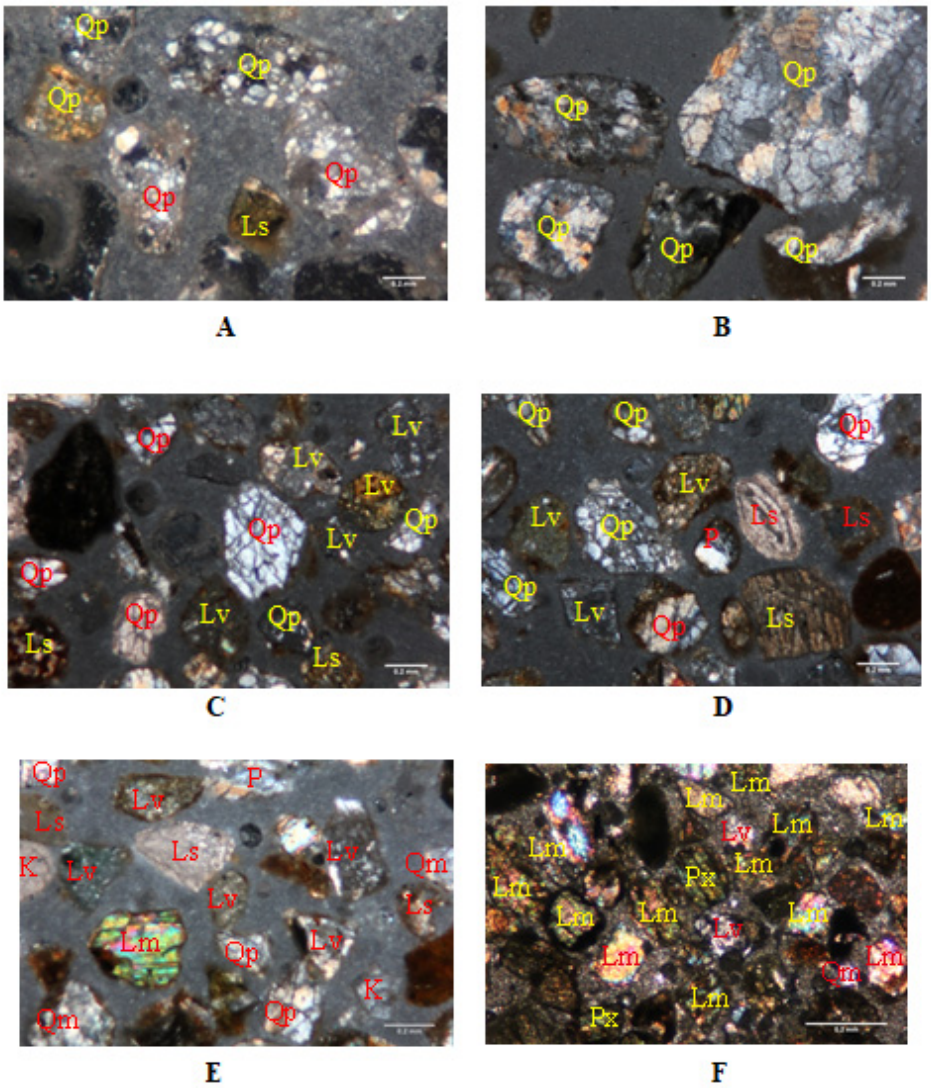

Figure 16. (A) Thin sections of TS deposit at SS-13, (B) TS deposit at SS-14, (C) modern beach sand at SS-13, (D) modern beach sand at SS-14, (E) fluvial sand in the mouth of Fengbin River close with SS-13 and SS-14, (F) modern fluvial sand in the Fengbin river. Qp: polycrystalline quartz, Qm: monocrystalline quartz, Lv: volcanic rock fragment, Lm: metamorphic rock fragment, Ls: sedimentary rock fragment, K: K-feldspar, P: plagioclase, and B: biotite

The TS deposit sorting is categorized as very poorly sorted, skewness includes in the near-symmetrical classification, and kurtosis shows very platykurtic (Table 10) (Folk & Ward, 1957).

The explanation of them is the source of sediments derived from a single source that contains highly grain size distribution. Therefore, the percentage of grain size is widely distributed. Based on the shape of the curve, the transport mechanism is dominated by saltation.

TS deposits at SS-13 and SS14 also contains some planktonic and benthic foraminifera fossils shown in figure 19. *Pulleniatina Obliquiloculata* and *Sphaerodinella dehiscens* (Fig. 19 A and B) reveal Quaternary Period. It can be interpreted that the deposition of this deposit occurred in the Quaternary Period. There are five species of benthic foraminifera discovered at SS-13 and SS-14, namely *Pseudorotalia schroeteriana*, *Quinqueloculina cuvieriana*, *Triloculina tricarinata*, *Bulimina sp*., and *Uvigerina peregrina*. Their living environment is in shallow marine with a depth approximately 30-100 m below sea-level (Hatta & Ujiie, 1992).

Petrographic analysis of TS deposits, modern beach sand deposits, and fluvial sand deposits at SS-1, SS-13, and SS-14 shows that compositions of quartz and rock fragments are more dominant than feldspar. TS deposits and modern beach sand deposits have almost the same characteristics. Their compositions are dominated by polycrystalline quartz and sedimentary rock fragments.

Table 8. the sorting, skewness, and kurtosis show very poorly sorted, near-symmetrical skewed, and very platykurtic

Mθ.f	(Mθ-x)	$(Mθ-x)^2$	$f.(Mθ-x)^2$	$(Mθ-x)^3$	$f.(Mθ-x)^3$	$(Mθ-x)^4$	$f.(Mθ-x)^4$
38.43813	1.706590909	2.912452531	31.98549509	4.970365013	54.58615515	8.482379745	93.15623614
95.41667	0.706590909	0.499270713	19.05549887	0.352780147	13.46444227	0.249271245	12.25142989
30.09091	-0.293409091	0.086088895	1.726995401	-0.025259264	-0.506716151	0.007411298	0.512932925
15.3952	-1.293409091	1.672907076	51.50948481	-2.163753221	-66.62283592	2.798618086	279.8618086
Total							
179.3409		Total	104.2774742		0.921045355		385.7824076
1.793409		Total/10	10.42774742		0.092104536		38.57824076
Sorting	3.229202288	33.67330582	108.7379162				
		3367.330582	10873.79162				
Skewness	0.016538558						
Kurtosis	0.035478187						

Table 9. The grain classification of the TS deposits at SS-14 is medium sand

Site	Grain Classification	Diameter (mm)	Diameter Phi (Φ)	Mid point (Mθ)	Frequency (gr)	Frequency (%)	Cumulative (%)
SS-1		0.0625	4				
SS-1	Very fine sand			3.5	20.67	12.04966772	12.04966772
SS-1		0.125	3				
SS-1	Fine sand			2.5	50.73	29.57327737	41.62294509
SS-1		0.25	2				
SS-1	Medium sand			1.5	63.08	36.77276437	78.39570946
SS-1		0.5	1				
SS-1	Coarse sand			0.5	37.06	21.60429054	100
		1	0				
Total					171.54	100	

Table 10. The sorting, skewness, and kurtosis are described as very poorly sorted, near-symmetrical skewed, and very platykurtic

Mθ.f	(Mθ-x)	$(Mθ-x)^2$	$f.(Mθ-x)^2$	$(Mθ-x)^3$	$f.(Mθ-x)^3$	$(Mθ-x)^4$	$f.(Mθ-x)^4$
42.173837	1.679316777	2.820104839	33.98132623	4.73584937	57.06541126	7.952991303	95.83090255
73.933193	0.679316777	0.461471284	13.64721828	0.313485186	9.270784345	0.212955746	8.863845323
55.159147	-0.320683223	0.102837729	3.781627586	-0.032978334	-1.21270452	0.010575599	0.829081552
10.802145	-1.320683223	1.744204174	37.68229375	-2.30354119	-49.7663731	3.042248202	304.2248202
Total							
182.06832		Total	89.09246585		15.35711794		409.7486496
1.8206832		Total/10	8.909246585		1.535711794		40.97486496
Sorting	2.984836107	26.59264089	79.37467472				
		2659.264089	7937.467472				
Skewness	0.075993094						
Kurtosis	0.051622089						

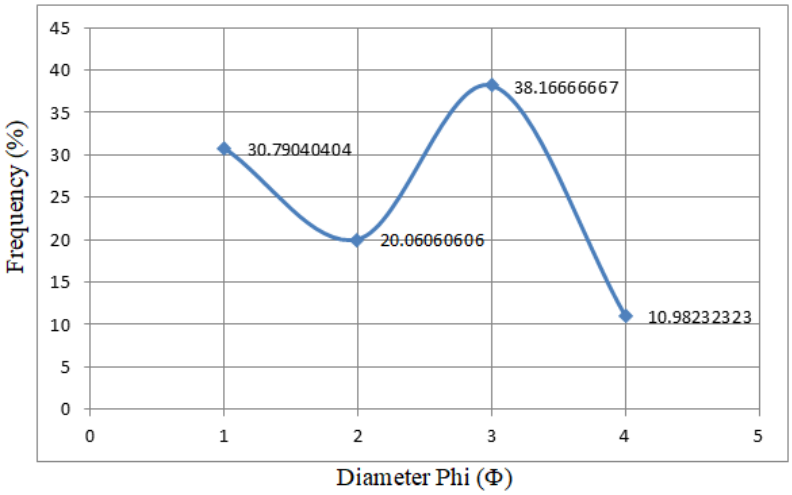

Figure 17. Grain size distribution curve of TS deposit at SS-13. It represents unimodal curve

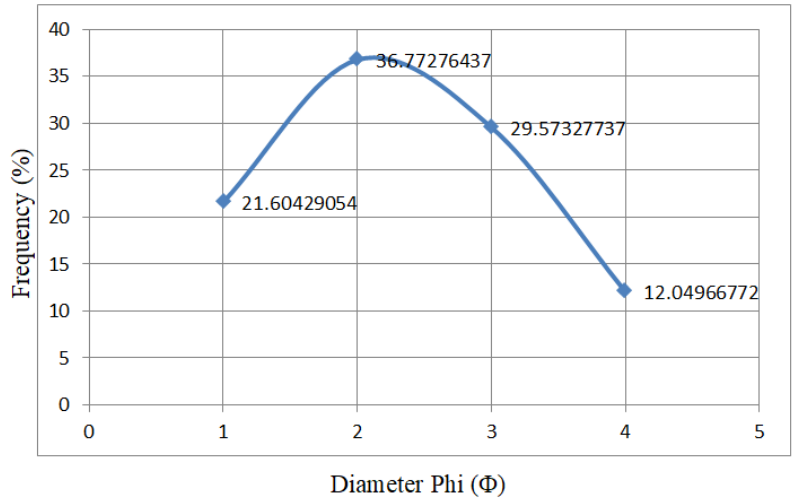

Figure 18. Grain size distribution curve of TS deposit at SS-14. It depicts unimodal curve

Whereas fluvial sand deposits are predominant monocrystalline quartz, volcanic and metamorphic fragments. Fluvial sand deposit samples are collected from the mouth of Fengbin and Fuyuan Rivers (Fig. 2). Table and triangle diagram of sand counting analysis according to Gazzi-Dickinson (1985) are shown in Table 11 and Figure 20 below this. Figure 20 exhibits that the type of sand in tsunami, beach, and fluvial deposits is litharenite. It is commonly found in orogenic Belts and associated with the deposition process in the delta.

Overall, 266 species of planktonic foraminifera and 702 benthic foraminifera species are identified. About 62% of planktonic foraminifera and 48% of benthic foraminifera show iron staining. Biozonation analysis of TS deposit (Table 12) indicates that the relative age of planktonic foraminifera is Quaternary Period (Pleistocene to Holocene) or 1.8 Ma-recent. Such relative age analysis is precise with absolute age estimation. Carbon dating represents that the age of beach gravel deposit in the lower part is 2340-2490 yr BP (Hsieh *et al*., 2011). Whereas TS deposits exist in the upper part of beach gravel deposit. Therefore, the estimation of absolute age for TS deposits in Changbin and Tulan marine terraces is less than 1 ka.

Table 11. Table of quartz (Q), feldspar (F), and rock fragment (L) percentages in TS deposits (ts), modern beach sand deposits (bs), and fluvial sand deposits (fs) in Fengbin

Sample	Percentage			Area
	Q (%)	F (%)	L (%)	
bs-1	56.27	3.45	40.28	Fengbin
bs-2	61.26	1.9	36.84	Fengbin
ts-1	62.67	4.89	32.44	Fengbin
ts-2	60.23	3.64	36.13	Fengbin
fs-1	33.25	3.55	63.2	Fengbin
fs-2	43.55	1.6	54.85	Fengbin

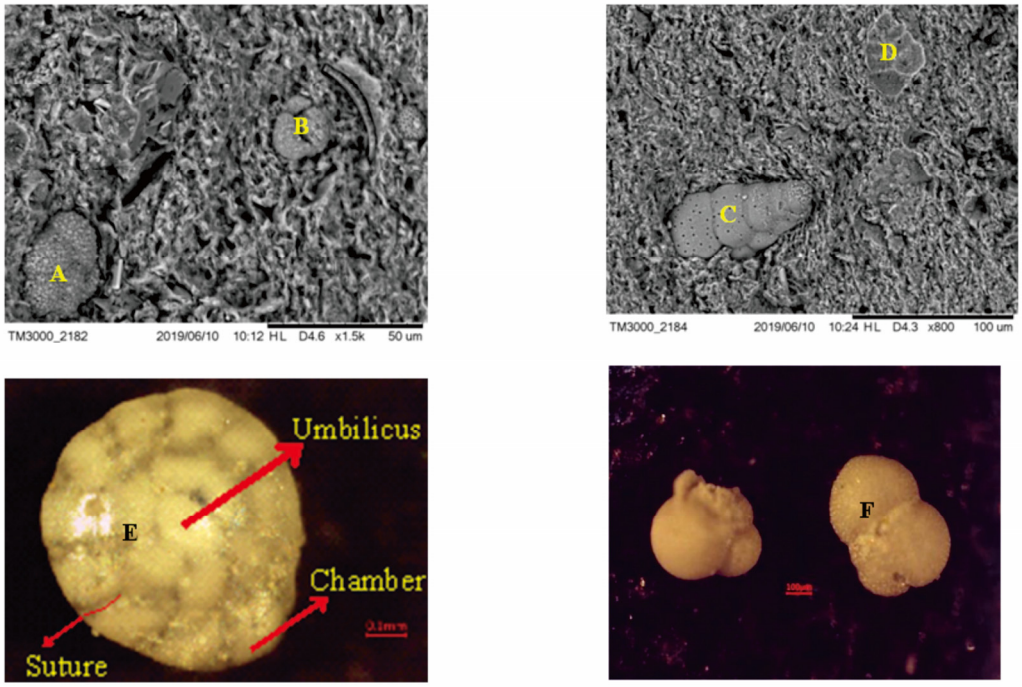

Figure 19. (A) Planktonic foraminifera *Pulleniatina obliquiloculata,* (B) *Sphaerodinella dehiscens,* (C) Benthic Foraminifera *Bulimina Sp.,* (D) *Uvigerina peregrina*, (E) *Pseudorotalia schroeteriana,* (F) *Trilobatus sacculifer*

Table 12. Biozonation analysis reveals that the age of TS deposits in Fengbin marine terrace is Quaternary Period (Pleistocene to Holocene)

Age	Description	Symbol & Thickness	Sample Code	Planktonic Zonation Postuma (1971)	Fengbin					
					Orbulina universa	*Trilobatus sacculifer*	*Pulleniatina obliquiloculata*	*Neogloboquadrina incompta*	Biodatum	Foraminifera Zonation
QUATERNARY	Fine sand	0 cm TS deposit 9 cm	S-5	N22	●	●	●	●	FO of *Pulleniatina obliquiloculata*	Interval zone of *Pulleniatina obliquiloculata*
			S-4		●	●	●	●		
	Medium sand	18 cm 27 cm	S-3		●	●	●	●		
			S-2		●	●	●	●		
PLIOCENE	Coarse Sand	36 cm 45 cm	S-1	N21	●	●		●		Assemblage zone of *Orbulina universa*, *Trilobatus sacculifer*, *Neogloboquadrina incompta*
Total					86	79	52	49		

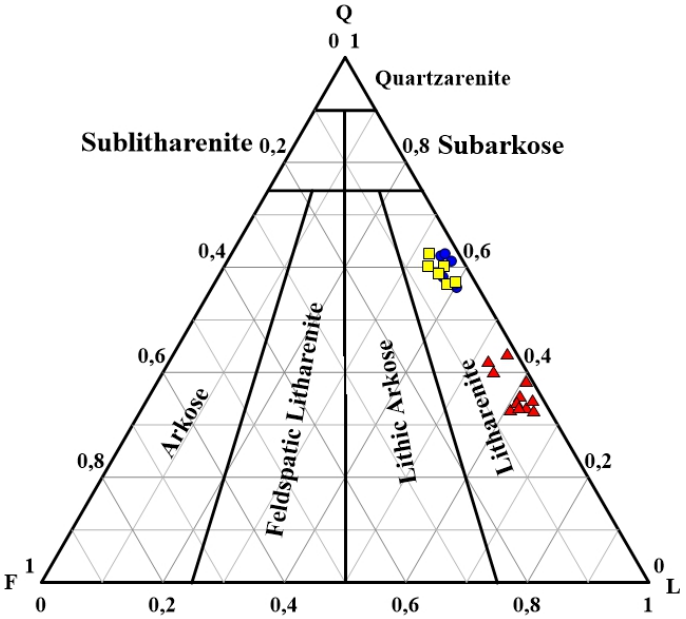

Figure 20. Sand counting triangle diagram above shows that the type of fluvial, modern beach, and TS sands are litharenite. Red triangle: fluvial sand which abundance of lithic (L), blue circle: modern beach sand that contain more dominant quartz (Q) than lithic, and yellow square: TS sand is dominated by polycrystalline quartz and sedimentary rock fragment. Fluvial, modern beach, and TS sands contain few feldspars (F)

Meanwhile, the age of beach gravel deposit in the upper part is around 1-2 ka. If TS deposit is created at less than 1 ka, this deposit may be associated with tsunami deposits in Ishigaki and Miyako Islands. It is because according to Ando et al. (2018), tsunami deposits in Ishigaki and Miyako Islands was generated at 248 yr BP and 920-620 yr BP.

The techniques used to divide the biostratigraphic zones are the assemblage zone of *Orbulina universa, Trilobatus sacculifer, Neogloboquadrina incompta*, and *Pulleniatina obliquiloculata*

interval zone (table 12). There are two biostratigraphic zonations based on table 12, namely *Neogloboquadrina incompta* zone in the bottom and *Pulleniatina obliquiloculata* zone in the top. *Neogloboquadrina incompta* zone is the Pliocene age (N21) characterized by *Neogloboquadrina incompta*, *Orbulina universa*, and *trilobatus sacculifer* assemblages.

Table 13. Paleo-bathymetry analysis of TS deposits represents that benthic foraminifera are derived from middle Neritic or 30-100 m below sea-level (Hatta & Ujiie, 1992)

Paleobathymetri		Fengbin								
		Elphidium craticulatum	*Quinqueloculina auberiana*	*Triloculina tricarinata*	*Quinqueloculina cuvieriana*	*Amphistegina radiata*	*Pseudorotalia schroeteriana*	*Rotalinoides compressiusculs*	*Bulimina sp.*	*Uvigerina peregrina*
Non-Marine										
Littoral										
Neritic	Inner									
	Middle									
	Outer									
Bathyal	Upper									
	Middle									
	Lower									
Total		156	4	46	168	16	126	18	89	79

$$\%P/B = \frac{P}{(P+B)}.100\% = \frac{266}{(266+702)}.100\% = 27.5\% \text{ (middle shelf)}$$

In the top of the *Neogloboquadrina incompta* zone, there is a *Pulleniatina obliquiloculata* zone which is Quaternary age and characterized by the first occurrence (FO) of *Pulleniatina obliquiloculata* fossils in the upper S-2 sample (Postuma, 1971). Based on the paleo-bathymetry analysis (Table 13), benthic foraminifera of TS deposit in Fengbin marine terrace is derived from middle Neritic or 30-100 m under sea-level (Hatta & Ujiie, 1992). It is based on shallow marine shell and coral boulder contents in this deposit. The sequence of stratigraphy is also described as coarsening upward which is the result of depositional when the regression occurred.

This result is similar to the result of marine shells analysis on tsunami deposits in Miyako and Ishigaki Islands. Ando et al. (2018) argued that marine shells contained on tsunami deposits in both islands are from middle neritic (30-100 m).

Generally, TS deposits have some specific characteristics, namely located at elevation between 10.5-12.5 m in Fengbin abundant shallow marine organisms, and predominantly sand-sized. The result of comparison of these deposits with modern beach sand and fluvial sand, then TS deposit tend to be more similar to modern beach sand. Therefore, the first conclusion is TS deposits are generated in the submarine environment. There are three possibilities concerning the origin of these deposits. The first assumption is these deposits are generated by transgression, so that very likely shallow marine organisms were deposited in these deposits. The second assumption is these deposits are formed by storm waves transported shallow marine organisms from offshore to onshore. The third assumption is tsunami waves carried shallow marine organisms from offshore to onshore.

According to Chen & Liu (1996, 2000), the mean sea-level between 0.2-1 ka is 1-2 m above the modern sea-level. The median mean sea-level at that time is 1.5 m above the modern sea-level. The uplift rate of marine terraces in Fengbin is 5 mm/yr (Hsieh *et al*., 2004). Therefore, the estimation of TS deposits elevation at that time in Fengbin is 4-6 m. Therefore, the first assumption is not eligible. Additionally, TS deposits in Fengbin is predominantly poorly sorted, which reveals rapid deposition. Commonly, the deposition of sediment materials during transgression takes place slowly so that generated well-sorted deposit.

It is possible that TS deposit was created due to storm waves like the second assumption. However, rip-up clasts structure has never been found in any storm deposit studies. This occurred because storm wave energy was not enough to erode cohesive sediments in coastal environments. Moreover, The run-up of storm wave is never more than 4 m. Haiyan Typhoon is one of the most powerful phenomena of hurricanes in this decade, storm wave run-up is only between 3.5 to 4 m. So, it can be concluded that the second assumption is less acceptable to explain the mechanism of this deposit formation.

TS deposit has a specific sedimentary structure, which is rip-up clasts. In previous tsunami studies, this sedimentary structure is often used as an indicator to distinguish between tsunami and storm deposits (Abe, 1938; Zhou & Adams, 1985; Ando et al., 2018). Tsunami wave run-up can reach more than 4 m. Therefore, it can be deduced that TS deposit is a tsunami deposit. Generally, the flow depth of the tsunami is lower than the tsunami wave run-up. If tsunami wave run-up in Fengbin reaches 4-6 m, then tsunami flow depth is less than 4 m. The distance of the tsunami deposit to the shoreline is around 50 m. So, it can be interpreted that tsunami waves can reach at least 50 meters inland.

There is a correlation between tsunami deposits in this study with tsunami deposits found in Ishigaki and Miyako Islands. In Ishigaki and Miyako Islands there are four tsunami deposits in the last 2000 years. The age of two tsunami deposits is estimated at 248 yr BP and 920-620 yr BP. The age of tsunami deposits on the eastern coast of Taiwan is estimated at less than 1 ka. Besides, the characteristics of tsunami deposits in Miyako and Ishigaki Islands tend to have abundant shallow marine organisms and rip-up clasts structure. These are similar to tsunami deposits on the eastern coast of Taiwan. If the maximum run-up of tsunami waves in Miyako

and Ishigaki Islands can reach 30 m, hence likely tsunami waves can reach the eastern coast of Taiwan with a lower maximum run-up.

Previous studies have attempted to simulate the possibility of a big sea wave trigger on the eastern coast of Taiwan. Research conducted by Ando et al. (2013) shows that a big sea wave on the eastern coast of Taiwan like Ami folklore is triggered by a submarine landslide in Changbin High as the effect of tectonic movement on plate boundary megathrust in Ryukyu trench. The term big ocean wave was used because previously, the cause of the wave was unknown. After the research, the "tsunami" term began to be used to mention a big sea wave that occurred on the eastern coast of Taiwan as Ami tribe told. After the discovery of tsunami deposits in Ishigaki and Miyako Islands that were estimated as the result of tsunami waves with a maximum run-up around 30 meters. Ando et al. (2018) tried to re-simulate to find the trigger of such tsunami waves. The simulation was undertaken with estimated fault length 150 km, fault dip 12^{o}, fault strike 255^{o} parallel with trench axis, fault slip 16 m, and fault width 230 km. The results of this simulation show that tsunami waves are caused by Ryukyu trench plate boundary megathrust. If the age of tsunami deposits in Fengbin is identic to tsunami deposits in Ishigaki and Miyako Islands then likely the trigger of tsunami waves on the eastern coast of Taiwan is the same with Ishigaki and Miyako Islands. Submarine landslide at Changbin High will not be able to cause sea waves with run-up roughly 4-6 m due to there is longshore current along the eastern coast of Taiwan that will block the wave. If it reaches to the mainland, the tsunami wave run-up will be less than 4 m even just 1-2 m. According to Ando *et al*. (2018), Ryukyu trench earthquake can generate big sea waves capable of reaching the mainland in some surrounding islands including Taiwan with the recurrence interval of 100-1000 years. Ando *et al*. (2018) also estimate the recurrence interval of tsunami in Ishigaki and Miyako Islands is 600 years. If this is true, the recurrence interval of the tsunami on the eastern coast of Taiwan is also 600 years.

Figure 21 illustrates the stratigraphic column location on the topographic map. The distance between SS-1 and SS-14 is roughly 1.5 km. While the distance between the SS-14 and SS-13 is approximately 500 m. The stratigraphic column as shown in Fig. 22 displays that alluvial fan deposits up to fluvial gravel in Fengbin is created in the submarine environment precisely at nearshore.

It is based on shallow marine shell and coral boulder contents in this deposit. The sequence of stratigraphy is also described as coarsening upward which is the result of depositional when the regression occurred.

Then the marine terrace underwent uplift with varying uplift rates coincide with the occurring mean sea-level drop. When the elevation of marine terrace reached about 4-6 m in Fengbin, a tsunami wave struck the eastern coast of Taiwan carrying sediments from offshore to the onshore.

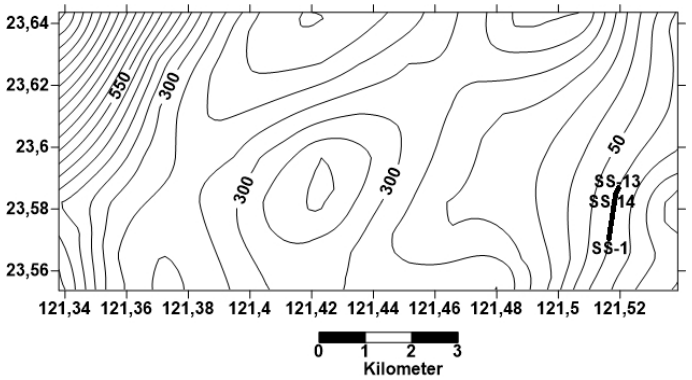

Figure 21. The topographic map depicts the location of stratigraphic column. SS-1: sampling site-1, SS-2: sampling site-2, SS-3: sampling site-3

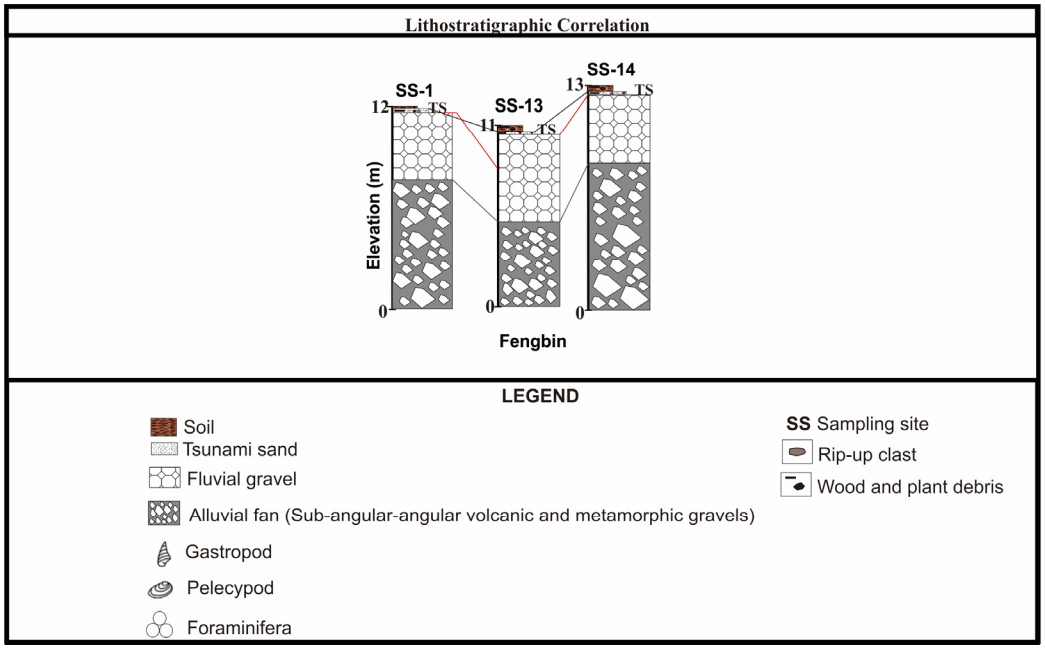

Figure 22. Lithostratigraphic column of marine terrace in Fengbin. TS deposits are above the fluvial gravel and below the soil. TS: Tsunami Sand (Hsieh et al., 2011)

Conclusions

Tsunami deposits on the marine terraces of Fengbin are at 10.5 to 12.5 m in elevation. The thickness of tsunami deposits in Fengbin varies around 15 to 20 cm. The main components of the tsunami deposit are polycrystalline quartz and sedimentary rock fragments. Meanwhile, granulometric analysis shows that the grain size classification of tsunami sediments is dominated by medium to coarse sand. Moreover, the erosional boundary with the underlying deposits was found in the tsunami deposit. This deposit has normal graded bedding (fining upward) and very poorly sorted.

Tsunami deposits are included in the *Pulleniatina obliquiloculata* zone which is Quaternary Period (Pleistocene-Holocene). The age determination of Quaternary Period is based on the first appearance of the *Pulleniatina obliquiloculata* planktonic foraminifera fossil in the S-2 sample code. The first occurence of *Pulleniatina obliquiloculata* is in the Quaternary Period (N22). Meanwhile, based on carbon dating, the absolute age of tsunami sediments is estimated at less than 1 ka. The results of the paleo-bathymetry analysis exhibit that benthic foraminifera of tsunami deposits originated from middle Neritic (30-100 m) below sea-level. The combination of uplift rate data, sea-level changes, and elevation where tsunami deposits are found illustrate that The height of the tsunami run-up is estimated 4 to 6 meters with an inundation distance of at least 50 m inland. The trigger of tsunami waves on the eastern coast of Taiwan is thought to originate from the Ryukyu trench plate boundary megathrust. Eventually, investigation of tsunami deposits on the eastern coast of Taiwan is somewhat difficult because the topography of marine terrace along Fengbin is rather steep in slope. Due to the lack of carbon dating data and the evidence of tsunami events are not well preserved, then the description of flow depth, inundation distance, and run-up of tsunami waves are less precise.

References

Abe, Y., 1938. The research of locality names in Taiwan. Sugita Publication, 300.

Ando, M., 1975. Source mechanisms and tectonic significance of historical earthquakes along the

Nankai Trough, Japan. Tectonophysics, 27: 119-140.
Ando, M., Nakamura, M., and Lin, C.H., 2013. Tsunami folklore and possible tsunami source on the eastern coast of Taiwan. Terrestrial, Atmospheric, and Oceanic Sciences, 24: 951-961.
Ando, M., Kitamura, A., Tu, Y., Ohashi, Y., Imai, T., Nakamura, M., Ikuta, R., Miyairi, Y., Yokoyama, Y., Shishikura, M., 2018. Source of high tsunamis along the southernmost Ryukyu trench inferred from tsunami stratigraphy. Tectonophysics, 722: 265-276.
Biq, C.C., 1972. Transcurrent buckling, transform faulting and transpression: their relevance in eastern Taiwan kinematics. Petroleum Geology of Taiwan, 10: 1-10.
Chen, C.S., 1988. Pliocene to Pleistocene biostratigraphical study in the Taiyuan area, Coastal Range, eastern Taiwan. Unpublished master thesis, National Taiwan University, Taipei, Taiwan.
Chen, C.S., Chen, W.C., Tao, W.K., 2004. Characteristics of heavy summer rainfall in southwestern Taiwan in relation to orographic effects. Journal of the Meteorological Society of Japan, 82: 1521-1543 .
Chen, H.F., 1984. Crustal uplift and subsidence in Taiwan: an account based upon retriangulation results. Central Geological Survey of Taiwan, 3: 129-140.
Chen, W.S., Huang, M.T., Liu, T.K., 1991. Neotectonic significance of the Chimei fault in the Coastal Range, eastern Taiwan. Proceedings of the Geological Society of China, 34: 43-56.
Chen, W.S., Wang, Y., 1997. Geological map of Fengbin, scale 1/50,000. Central Geological Survey, Ministry of Economic Affairs, Taiwan .
Chen, Y.G., Liu, T.K., 1996. Sea-level changes in the last several thousand years, Penghu Islands, Taiwan Strait. Quaternary Research, 45: 254-262.
Chen, Y.G., Liu, T.K., 2000. Holocene uplift and subsidence along an active tectonic margin, southwestern Taiwan. Quaternary Science Reviews, 19: 923-930.
Chi, W.R., Namson, J., Suppe, J., 1981. Record of plate interactions in the Coastal Range, eastern Taiwan. Petroleum Geology of Taiwan, 17: 75-87.
Cole, R.B., Stanley, R.G., 1994. Sedimentology of subaqueous volcaniclastic sediment gravity flows in the Neogene Santa Maria Basin, California. Geological Society of America Bulletin, 103: 221-235.
Dickinson, W.R., 1985. Interpreting provenance relation from detrital modes of sandstones. Reidel Publishing Company, 333-363.
Dolozi, M.B., Ayres, L.D., 1991. Early Proterozoic, basaltic andesite tuff-breccia: downslope, subaqueous mass transport of phreatomagmatically-generated tephra: Bulletin of Volcanology, 53: 477-495.
Dorsey, R.J., 1985. Petrography of Neogene sandstones from the Coastal Range of eastern Taiwan, Response to arc-continent collision: Petrography of Neogene sandstones from the Coastal Range of eastern Taiwan. Petroleum Geology of Taiwan, 21: 187-216.
Dorsey, R.J., 1992. Collapse of the Luzon volcanic arc during onset of arc-continent collision: evidence from a Miocene-Pliocene uncomformity, eastern Taiwan. Tectonics, 11: 177-191.
Ernst, W.G., 1983. Mountain-building and metamorphism: a case history from Taiwan. Academic Press, London, 247-256.
Falade, F., Ikponmwosa, E.E., Ojediran, N.I., 2010. Behaviour of lightweight concrete containing periwinkle shells at elevated temperature. Journal of Engineering Science and Technology, 5: 379-390.
Fisher, R.V., and Schmincke, H.U., 1984. Pyroclastic rocks. Springer-Verlag, Berlin Heidelberg, 427.
Folk, R. L., Ward, W. C., 1957. Brazos river basin: A study in the significance of grain size parameter. Journal of Sedimentary Petrology, 27: 3-27.
Fujiwara, O., 2008. Bedforms and sedimentary structures characterizing tsunami deposits. Tsunamiites, 10: 51-62.
Ge, X., Li, T., Zhang, S., Peng, M., 2010. What causes the extremely heavy rainfall in Taiwan during typhoon morakot (2009)?. Atmospheric Science Letter, 11: 46-50 .
Hatta, A., Ujiie, H., 1992. Benthic foraminifera from Coral Seas between Ishigaki and Iriomote Islands, southern Ryukyu Island Arc, northwestern Pacific. Systematic descriptions of Rotaliina. Bulletin of the College of Science, University of the Ryukyus, 54: 163-287.
Hewitt, K., 2002. Styles of rock avalanche depositional complexes conditioned by very rugged terrain, Karakoram Himalaya, Pakistan. Geological Society of America Reviews in Engineering Geology XV, Boulder, Colorado, 345-377.

Ho, C.S., 1986. A synthesis of the geologic evolution of Taiwan. Tectonopysics, 125: 1-16 .
Hsieh, M.L., 1990. Study of late Quaternary deposits, marine terraces and neotectonism of the coastal area between Hualien and Taitung. Master thesis, Institute of Geology, National Taiwan University, Taipei.
Hsieh, M.L., Liew, P.M., Chen, H.-W., 2011. Early Holocene catastrophic mass-wasting event and fan-delta development on the Hua-tung coast, eastern Taiwan. Geomorphology, 134: 378-393.
Hsieh, M.L., Liew, P.M., Hsu, M.-Y. 2004. Holocene tectonic uplift on the Hua-tung coast, eastern Taiwan. Quarternary International, 115: 47-70.
Hsieh, M.L., Rau, R.J., 2009. Late Holocene coseismic uplift on the Hua-tung coast, eastern Taiwan: evidence from mass mortality of intertidal organisms. Tectonophysics, 474: 595-609.
Hsin, Y.C., Wu, C.R., Shaw, P.T., 2008. Spatial and temporal variations of the Kuroshio east of Taiwan, 1982-2005: a numerical study. Journal of Geophysical Resources, 113.
Hsu, M.Y., Kao, C.J., Kao, P.F., Jeng, S.L., 1999. A study of coastal retreat along Huatung Coast, Hualien to Changbin section. Bulletin of Geographical Society of China, 27: 83-109.
Hsu, T.L., 1956. Geology of the Coastal Range, eastern Taiwan. Bulletin of Geological Survey of Taiwan, 8: 39-63.
Hsu, T.L., Kao, C.J., Kao, P,F., Jeng, S.L., 1998. A study of coastal retreat along Huatung Coast, Hualien to Changbin section. Bulletin of Geographical Society of China, 26: 73-98.
Huang, T.Y., 1969. Some planktonic foraminifera from a bore at Shihshan, near Taitung, Taiwan. Proceedings Geological Society of China, 12: 103-119.
Hunter, R.E., 1980. Depositional environments of some Pleistocene coastal terrace deposits, southwestern Oregon-case history of a progradational beach and dune sequence. Sedimentary Geology, 27: 241-262.
International Society of Rock Mechanics, 1978. Committee on standardization of laboratory and field tests. Suggested methods for the quantitative description of discontinuities in rock masses. International Journal of Rock Mechanics Science and Geomechanics Abstract, 15: 319-368.
Jahn, B.M., Liou, J.G., Nagasawara, H., 1981. High-pressure metamorphic rocks of Taiwan. REE geochemistry, Rb-Sr ages and tectonic implications. Metamorphic Geological Society of China, 4: 497-520.
Jian, Z., Wang, P., Saito, Y., Wang, J., Pflaumann, U., Oba, T., Cheng, X., 2000. Holocene Variability of the Kuroshio Current in the Okinawa Trough, northwest Pacific Ocean. Earth Planet Science Letter, 184: 305-319 .
Lallemand, S., Theunissen, T., Schnurle, P., Le, C.S., Font, Y., 2013. Indentation of the Philippine Sea Plate by the Eurasia Plate in: details from recent marine seismological experiments. Tectonophysics, 594: 60-79 .
Lallemand, S., Lehu, R., Retif, F., Hsu, S.K., Babonneau, N., Ratzov, G., 2016. A~3000 years-old sequence of extreme events revealed by marine and shore deposits east of Taiwan. Tectonophysics, 692: 325-341.
Lau, A.Y.A., Switzer, A.D., Domincy-Howes, D., Aitchison, J.C., Zong, Y., 2010. Written records of historical tsunamis in the northeastern South China Sea challenges associated with developing a new integrated database. Natural Hazards Earth System Sciences, 10: 1793-1806 .
Lehu, R., Lallemand, S., Hsu, S.K., Lin, A.T., Ratzov, G., Babonneau, N., Dezileau, L., 2013. Submarine paleoseismology offshore Taiwan: new insights from turbidite records. Abstract in AGU Fall Meeting.
Lehu, R., Lallemand, S., Hsu, S.K., Babonneau, N., Ratzov, G., Lin, A., 2015. Deep-sea sedimentation offshore eastern Taiwan: facies and processes characterization. Marine Geology, 369: 1-18.
Lehu, R., Lallemand, S., Ratzov, G., Babonneau, N., Hsu, S.K., Lin, A., 2016. An attempt to reconstruct 2700 years of seismicity using deep-sea turbidites offshore eastern Taiwan. Tectonophysics, 5: 16-34.
Lieu. J.G., Ernst, W.G., 1984. Summary of Phanerozoic metamorphism in Taiwan. Metamorphic Geological Society of China, 133-152.
Liew, P.M., Hsieh, M.L., Lai, C.K., 1990. Tectonic significance of Holocene marine terraces in the Coastal Range, eastern Taiwan. Tectonophysics, 183: 121-127.
Liew, P.M., Pirazzoli, P.A., Hsieh, M.L., Arnold, M., Barusseau, J.P., Fontugne, M., 1993. Holocene tectonic uplift deduced from elevated shorelines, eastern Coastal Range of Taiwan. Tectonophysics,

222: 55-68.
Liu, J., Liu, C., Xu, K., Milliman, J., Chiu, J., Kao, S., Lin, S., 2008. Flux and fate of small mountainous rivers derived sediments into the Taiwan Strait. Marine Geology, 256: 65-76.
Liu, Y.C., Yu, S.B., 1990. Vertical crustal movements in eastern Taiwan and their tectonic implications. Tectonophysics, 183: 111-120.
Ma, K.F., Lee, M.F., 1997. Simulation of historical tsunamis in the Taiwan region. Terrestrial Atmospheric and Oceanic Sciences, 8: 13-30.
Malavieille, J., Lallemand, S.E., Dominguez, S., Deschamps, A., Lu, C.Y., Liu, C.S., Schnurle, P., 2002. Arc-continent collision in Taiwan: new marine observations and tectonic evolution. Geological Society of America, 358: 187-211.
Massari, F., Parea, G.C., 1988. Progradational gravel beach sequences in a moderate to high energy, microtidal marine environment. Sedimentology, 35: 881-913.
Matta, N., Chen, W.S., Nishikawa, Y., Ando, M., Chung, L.H., 2013. Finding of probable tsunami boulders on Jiupeng coast in southeastern Taiwan. Terrestrial, Atmospheric and Oceanic Sciences, 24: 159-163.
Morton, R.A., Gelfenbaum , G., Jaffe, B.E., 2007. Physical criteria for distinguishing sandy tsunami and storm deposits using modern examples. Sedimentary Geology, 200: 184-207.
Nemec, W., Steel, R.J., 1984. Alluvial and coastal conglomerates: their significant features and some comments on gravelly mass-flow deposits. Canadian Society of Petroleum Geologist Memoir 10, Calgary, Alberta, 1-31.
Ota, Y., Shyu, B., Wang, C.C., Lee, H.C., Chung, L.H., Shen, C.C., 2015. Coral boulders along the coast of the Lanyu Island, offshore southeastern Taiwan, as potential paleotsunami records. Journal of Asian Earth Sciences, 114: 588-600.
Postma, G., 1983. Water escape structures in the context of depositional model of a mass flow dominated conglomeratic fan-delta (Abrioja Formation, Pliocene, Almeria Basin, SE Spain). Sedimentology, 30: 91-103.
Postuma, J., 1971. Manual of Planktonic Foraminifer. Elsevier Publishing Company, 420 .
Putra, P.S., 2018. Tsunami sediments and their grain size characteristics. IOP Conference Series: Earth and Environmental Science, 118 .
Ramsey, L.A., Hovius, N., Lague, D., Liu, C.S., 2006. Topographic characteristics of the submarine Taiwan orogen. Journal of Geophysical Resources, 111.
Sarkar, D., Mukhopadhyay, A., Hazra, S., 2013. Characteristics of tsunami and paleo Tsunami deposits in South Andaman Island, India. Indian Journal of Geo-Marine Sciences, 42: 839-848 .
Sohn, Y.K., Kim, S.B., Hwang, I.G., Bahk, J.J., Choe, M.Y., Chough, S.K., 1997. Characteristics and depositional processes of large-scale gravelly Gilbert-type foresets in the Miocene Doumsan fan delta, Pohang Basin, SE Korea. Journal of Sedimentary Research, 67: 130-141.
Suppe, J., 1984. Kinematics of arc-continent collision, flipping of subduction, and back-arc spreading near Taiwan. Metamorphic Geological Society of China, 6: 21-33 .
Teng, L.S., 1979. Petrographical study of the Neogene sandstones of the Fenshuliao Formation, northern Coastal Range, eastern Taiwan. Acta Geology Taiwanica, 20: 129-155.
Teng, L.S., 1990. Geotectonic evolution of the late Cenozoic arc-continent collision in Taiwan. Tectonophysics, 183: 57-76 .
Theunissen, T., Font, Y., Lallemand, S., Liang, W.T., 2010. The largest instrumentally recorded earthquake in Taiwan: revised location and magnitude, and tectonic significance of the 1920 event. Geophysical Journal International, 183: 1119-1133.
Ujiie, Y., Ujiie, H., Taira, A., Nakamura, T., Oguri, K., 2003. Spatial and temporal variability of surface water in the Kuroshio source region, Pacific Ocean, over the past 21,000 years: evidence from planktonic foraminifera. Marine Micropaleontology, 49: 335-364 .
Wang, U., Yang, C.N., Chen, W.S., 1992. Geological map of Yuli. Central Geological Survey of Taiwan, scale 1:50,000.
Wijaya, E., Abdurrokhim, Helmi, F., Ilmi, N.N., Sunardi, E., 2017. Lithofacies and depositional environment of Halang Formation on part of Chikeu river section, Majalengka, North Java. Journal of Geological Sciences and Applied Geology, 2: 17-27 .
Yamaguchi, M., Ota, Y., 2004. Tectonic interpretations of holocene marine terraces, east coast of Coastal Range, Taiwan. Quaternary International, 115: 71-81.

Yen, T.P., Sheng, C.C., Keng, W.P., 1951. The discovery of fusuline limestone in the metamorphic complex of Taiwan. Bulletin Geological Survey of Taiwan, 3: 23-25.
Yen, T.P., 1967. Structural analysis of the Tananao Schist of Taiwan. Bulletin of the Geological Survey of Taiwan, 18: l-110.
Yu, N.T., Yen, J.Y., Chen, W.S., Yen, I.C., Liu, J.H., 2015. Geological records of western pacific tsunamis in northern Taiwan: AD 1867 and earlier event deposits. Marine Geology, 372: 1-16.
Zhou, Q., Adams, W.M., 1985. Tsunamigenic earthquakes in China 1831 B.C. - 1980 A.D. International Tsunami Symposium, 543-550.